2010

Model-based nonlinear control of active tilting-pad bearings

An Wu
Louisiana State University and Agricultural and Mechanical College, awu1@lsu.edu

MODEL-BASED NONLINEAR CONTROL OF ACTIVE TILTING-PAD BEARINGS

A Dissertation

submitted to the Graduate Faculty of the
Louisiana State University and
Agricultural and Mechanical College
in partial fulfillment of the
requirements for the degree of
Doctor of Philosophy

in

The Department of Mechanical Engineering

by
An Wu
B.S., Electrical Engineering, Huazhong University of Science and Technology, China, 2006
August, 2010

Acknowledgements

I would like to thank everybody who helped me finish this dissertation. I would like to thank Dr. de Queiroz, my advisor. Without his advising, I could not have completed my Ph.D. degree at all. I am especially thankful for his kindness, strictness on academic standards, and patience with my research progress. I also want to thank my committee members and especially Dr. Michael Martin for his advice and help. Finally, I want to thank my family for their support.

Table of Contents

List of Tables

List of Figures

Abstract

A promising mechanical bearing candidate for active operation is the tilting-pad bearing. The proposed active tilting-pad bearing has linear actuators that radially translate each pad. The use of feedback control in determining the actuator forces allows for the automatic, continuous adjustment of the pad position during the operation of the rotating machine. In the first part of the dissertation, we develop a nonlinear dynamic model of the active bearing system. The hydrodynamic force produced by the fluid film is modeled as a nonlinear, squeeze-film damper plus repellent spring. A model-based nonlinear controller is then designed to exponentially regulate the rotor position to the origin. A proof-of-concept experiment shows that the active strategy improves the bearing performance relative to its traditional passive operation. Further, the experiment demonstrates that the model-based nonlinear control regulates the rotor comparably to a linear PID control, but requires significantly less control energy.

The second part of the dissertation introduces a new type of active fluid-film bearing which actively adjusts the angular velocity of the pads of a tilting-pad bearing. This is motivated by the observation that there is more control authority in the pad tilting motion than in its radial translation. To this end, a dynamic model for the bearing system is developed, inclusive of the nonlinear hydrodynamic force for the infinitely-short bearing case. A model-based controller is then constructed, based on measurements of the journal position and velocity and pad tilting angles, to ensure that the journal is asymptotically regulated to the bearing center. Numerical simulations illustrate the performance of the active bearing under the proposed control in comparison with the bearing's standard passive mode of operation.

Chapter 1 Introduction

Traditional mechanical bearings, such as rolling element and fluid film bearings, are passive devices in the sense that they cannot adjust their dynamic behavior in response to changes in the operating conditions of the system. To overcome this deficiency, *active* bearings have been proposed to improve the stability and performance of the rotating machine. Active bearings can eliminate rotor vibration through active damping, adjust the load stiffness, provide an automatic rotor balancing capability, and compensate for misalignment and changes in rotor speed. Magnetic bearings are the most popular type of active bearing, and have been a subject of extensive research. Magnetic bearings are well suited for high-speed applications because, due to their non-contact nature, they have the unique ability to suspend loads with no friction. However, due to their low load-carrying capacity and high cost relative to mechanical bearings, magnetic bearings are not the most cost-effective solution for many low to medium speed, high-load applications. In addition, since magnetic bearings are open-loop unstable (i.e., when operated with no feedback control), they require backup ball bearings in the event of a magnetic bearing failure.

The ability to control magnetic bearings is generating an increasing interest in adapting traditional mechanical bearings for active use. The *tilting-pad bearing* is one promising journal bearing candidate for active operation. In fact, an economical feasibility and technological assessment report prepared for the Electric Power Research Institute identified this class of bearing as one of the best suited for active control in power plants [1]. A *passive* tilting-pad bearing is a type of hydrodynamic bearing, containing a circumferential arrangement of pad segments supported by fixed pivots. A thin film of fluid is located in the gap between the journal and the pads. Each pad is free to tilt about its pivot in response to the rotor motion. As the pads tilt, they vary the geometry and thickness of the fluid film, which then exerts a stabilizing hydrodynamic

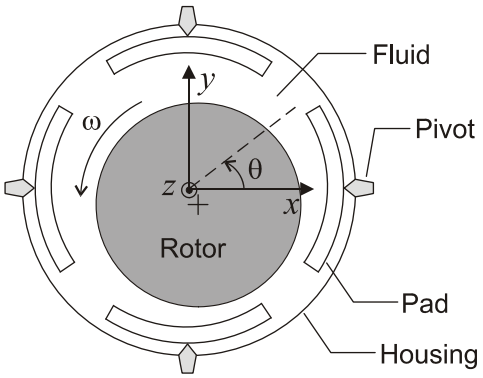

Figure 1.1: Schematic representation of the tilting-pad bearing.

force on the rotor. Therefore, unlike the magnetic bearing, the passive tilting-pad bearing can have a stable open-loop operation [6]. See Figure 1.1 for an illustration of a four-pad, tilting-pad bearing.

One approach for transforming the tilting-pad bearing into an active bearing is to actuate each pad along the radial direction. This idea, which was apparently introduced by [14], is akin to actively adjusting the tilting-pad bearing's preload factor [2]. The reasoning behind this approach can be understood from the Reynolds equation [8], which governs the pressure field within the bearing clearance:

$$\frac{1}{r^2}\frac{\partial}{\partial\theta}\left(h^3\frac{\partial p}{\partial\theta}\right)+\frac{\partial}{\partial z}\left(h^3\frac{\partial p}{\partial z}\right)=6\mu\omega\frac{\partial h}{\partial\theta}+12\mu\frac{\partial h}{\partial t} \tag{1.1}$$

where p is the pressure field between the journal and pads, θ and z are the angular and axial coordinates of the bearing system, respectively, h is the fluid film thickness, r is the journal radius, ω denotes the journal angular speed, and μ is the constant fluid viscosity. On the right-hand side of (1.1), the first and second terms are known as the physical wedge and normal squeeze effects, respectively [8]. The form of the normal squeeze term indicates that varying the film thickness in time provides a means of controlling the pressure field, in turn, affecting the load-carrying capacity and stability of the bearing. The variation of h in time can be directly accomplished by radially actuating the pads.

In the active system initially suggested in [14], the film thickness that optimized the system performance for a given journal speed was pre-determined by calculation or experimentation. This information was then used to translate the pads during operation through piezoelectric pushers depending on the journal speed. Note that this active system is open loop in the sense that the journal and pad displacements are not utilized to adjust the pads. In [13], another open-loop, active tilting-pad bearing was proposed by mounting the pads on flexible hydraulic chambers. The chamber pressure was changed via a proportional valve, resulting in a displacement of the pads. The pad positions that produced the desired bearing damping and stiffness coefficients were pre-determined off-line through the coefficients' dependency on the bearing clearance.

The first work to propose the adjustment of the fluid film thickness using feedback control was [5]. The motivation for the use of feedback is the ability to automatically adjust the pad position during the system operation based on measurements of the pad and journal motions. This can be accomplished by placing a linear actuator behind each pad to radially translate the pads without affecting the pad tilting motion. In [5], the hydrodynamic force produced by the movement of the pads against the fluid film was modeled as a linear spring plus damper. By assuming the stiffness and damping coefficients to be known about a given journal equilibrium state, the bearing system model was represented by a linear state-space equation with the pad radial velocities as control inputs. Later in [6], a linear quadratic regulator was proposed for the linear state-space model developed in [5]. In [3], the hydrodynamic force was modeled as a linear spring-damper with unknown damping and stiffness coefficients, and an adaptive feedback controller was designed to asymptotically regulate the journal displacement to the bearing center.

In Chapter 2 of this dissertation, we first expand upon the work of [3] by developing a *nonlinear* model for the hydrodynamic force in the tilting-pad bearing. This model is used in the equations of motion of the active tilting-pad bearing system with the control inputs being the forces

applied to each pad via actuators. The equations of motions are composed of the second-order dynamics of the rotor and the second-order dynamics of the pads, which are decoupled through the hydrodynamic force. The nonlinear model we propose for hydrodynamic force takes the form of a squeeze-film damper plus repellent spring. The key aspects of proposed bearing model are justified numerically and experimentally. We then construct a model-based nonlinear control law to stabilize the rotor at the center of the bearing system. Lyapunov theory is used to analyze the stability of the resulting closed-loop system. A proof-of-concept experimental study of the active tilting-pad bearing system is also presented. The objective of the experiment is twofold: (i) demonstrate that active control improves the performance of the tilting-pad bearing system relative to its traditional, passive mode of operation, and (ii) compare the controller based on the proposed nonlinear system model with a linear PID controller. To the best of our knowledge, this research is the first to report the experimental demonstration of an active tilting-pad bearing using feedback control.

In Chapter 3 of this dissertation, we depart from the existing choice of control input to the active tilting-pad bearing system (see above), and propose to utilize the pad *angular* velocities as inputs. The motivation for this new active method is the following. First, the wedge action in (1.1) has more pressure-generating capacity [8, 9] (and thus, more control authority over the journal motion) than the squeeze action. This fact is illustrated in the third chapter of this dissertation. Second, the pad tilting motion has a direct effect on the wedge action. Third, one can actively adjust the pad angular velocity via a *rotary* electric motor, which is generally less costly than its linear counterpart and piezo-actuators. In this chapter, the nonlinear equations of motion for the proposed active tilting-pad bearing system are derived first. The infinitely-short bearing assumption is then used to facilitate the calculation of the nonlinear hydrodynamic force. Next, a model-based nonlinear feedback control law for the pad angular velocities is designed to

stabilize the journal motion at the bearing center. Simulation results compare the performance of the proposed active method to the bearing's traditional passive operation.

Chapter 2 Tilting-Pad Bearing with Active Pad Translation

We revisit the active tilting-pad bearing system of [3], where each pad is translated along the radial direction. The goal is to develop a more accurate model more for the nonlinear hydrodynamic forces acting on the journal and then design a nonlinear feedback controller for the new system model.

2.1 Bearing System Model and Problem Statement

Consider the four-pad, active tilting-pad bearing system shown in Figure 2.1. Let (x, y, z) be an inertial coordinate frame with origin at the bearing geometric center. To model the system, we assume that: (i) the rotor shaft is vertical, (ii) the rotor, pivots, and pads are rigid, (iii) the motion of the rotor along the x and y directions are decoupled, and (iv) the rotor is spinning at a known, constant angular speed ω, (v) the fluid viscosity is constant, and (vi) a fluid film is always present between the journal and pads. Note that Assumption (iii) is motivated by the fact that tilting-pad bearings are known to minimize cross-coupling effects because of their ability to disrupt circumferential flows [2, 11, 15]. (More about this assumption later in Section 2.4.)

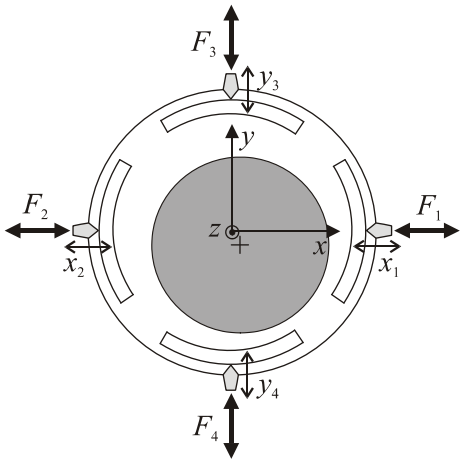

Figure 2.1: Tilting-pad bearing with active pad translation.

Due to Assumption (iii), we only present the model and control strategy for the x direction. To this end, let x_r, x_1, and x_2 denote the position of the journal, right pad, and left pad along the

x axis, respectively. Let m_r and m_i be the constant mass of the rotor and i-th pad, respectively. Finally, F_i denotes the control force applied to the i-th pad. The equations of motion for the rotor-bearing system are given by

$$m_r \ddot{x}_r = \sum_{i=1}^{2} f_{hi} \tag{2.1a}$$

$$m_i \ddot{x}_i = F_i - f_{hi}, \quad i = 1, 2 \tag{2.1b}$$

where f_{hi} is the hydrodynamic force the fluid film applies on the journal and i-th pad. To determine the hydrodynamic forces, one needs to solve the Reynolds equation (1.1) and then integrate the resulting pressure field over the journal contact area. Unfortunately, due to the nonlinear, two-dimensional nature of (1.1, a general closed-form expression for the hydrodynamic forces is not possible to obtain. As a result, a model that approximates the behavior of f_{hi} is required for the design of a control law. Typically, the following simple, linear model is used [3, 5, 6]

$$f_{hi} = \alpha_i \left(x_i - x_r \right) + \beta_i \left(\dot{x}_i - \dot{x}_r \right), \quad i = 1, 2 \tag{2.2}$$

where $\alpha_i, \beta_i > 0$ are constant, stiffness and damping coefficients, respectively. This model assumes the hydrodynamic force behaves like a standard, mechanical spring plus viscous damper. Rather, we propose the following nonlinear, repellent spring plus squeeze-film damper model for the hydrodynamic force

$$f_{hi} = \frac{a_i}{\left(x_r - x_i + (-1)^{i+1} r \right)^3} + \frac{(-1)^i b_i}{\left(x_r - x_i + (-1)^{i+1} r \right)^3} \left(\dot{x}_i - \dot{x}_r \right), \quad i = 1, 2 \tag{2.3}$$

where $a_i, b_i > 0$ are stiffness- and damping-related parameters, respectively, and r is the journal radius. The denominators in (2.3) will never become zero because, due to geometric/physical constraints in the bearing system and Assumption (vi) above, we have that $x_r - x_i > (-1)^i r$. In fact, $\left| x_r - x_i + (-1)^{i+1} r \right| = h_i$, i.e., the film thickness between the journal and the i-th pad.

The statement of our control objective is as follows. Given the nonlinear dynamics (2.1) and (2.3), design a model-based control law for F_i, $i = 1, 2$ that ensures $x_r(t), \dot{x}_r(t) \to 0$ as $t \to \infty$

and the boundedness of all signals, using feedback of x_r, $\dot{x}_r$, x_i, and $\dot{x}_i$, $i = 1, 2$. Due to the model-based nature of the control law to be developed, we present in Section 2.4 computational and experimental studies that justify the structure of the above model. We first though describe in the next two sections the numerical simulation and experimental test rig used to validate the proposed system model and feedback control.

2.2 Numerical Simulation

We developed a program for numerically calculating the hydrodynamic force of the tilting-pad bearing system with high fidelity. The program is based on the Reynolds equation for laminar, incompressible, Newtonian, inertialess, thin-film flows [8]. Specifically, we numerically solved the dimensionless form of the Reynolds equation for the pressure field between the rotor and pads with appropriate boundary conditions at the pad edges using the center differences method [7]. The pressure field was then numerically integrated along the surface area of each pad to give the *actual* hydrodynamic force acting on the pads (an equal but opposite force acts on the rotor). The hydrodynamic force depends on the oil viscosity, rotor angular speed, oil inlet pressure, and geometry of the fluid film. The fluid film geometry is a function of the displacement and translational velocity of the rotor and pads, pad tilt angle, pad arc, pad length, journal radius, and pad radius of curvature. All the above variables serve as inputs to the program, which after the necessary calculations outputs the hydrodynamic force in the bearing.

2.3 Experimental Test Rig

A test rig was designed and built [4] consisting of a rotor with a vertical axis of rotation, a tilting-pad bearings with four pads and a housing for the rotor/pads/lubricant assembly. Figure 2.2 shows a schematic drawing of the test rig and its main components, while a picture of the actual rig is shown in Figure 2.3. The pads, made of copper, were supported by a pusher and placed inside the reservoir. The pushers were connected to the pads through small holes in the reservoir. The pads were free to tilt about a pin. A picture of the pad/pivot assembly is given in Figure 2.4.

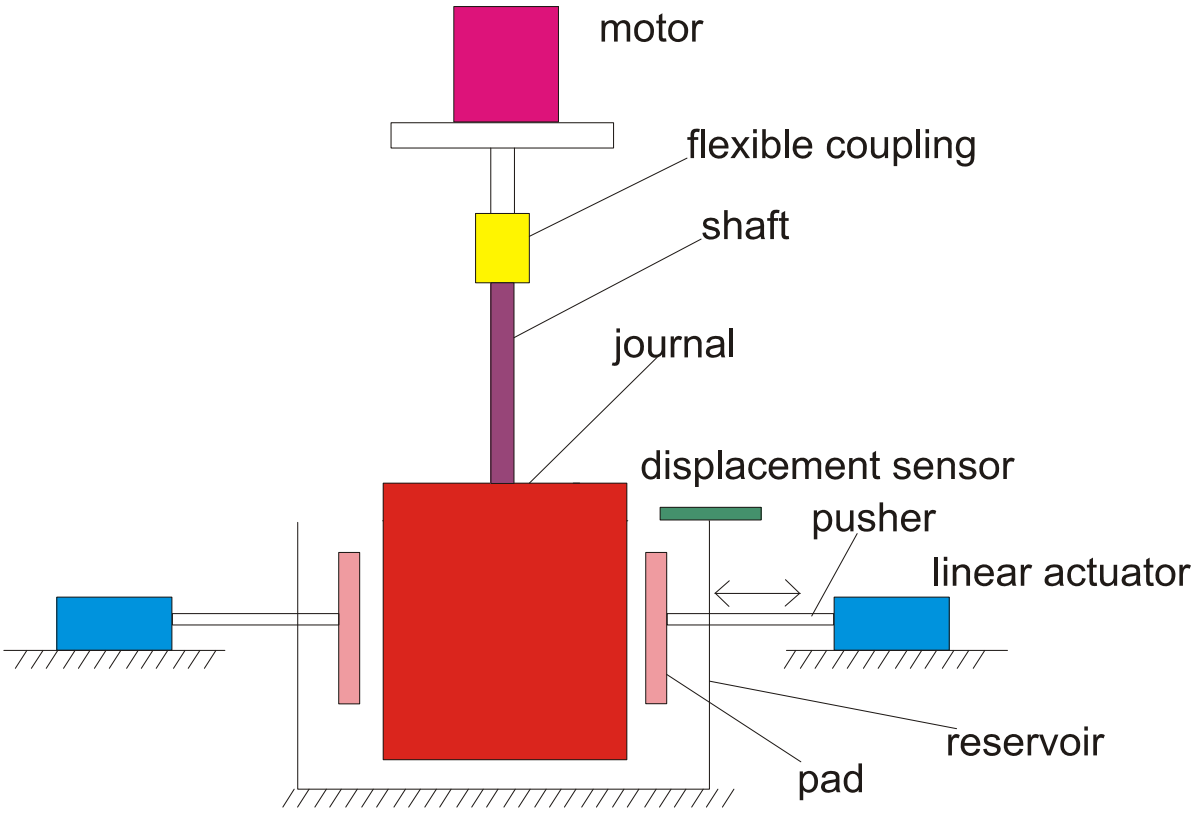

Figure 2.2: The schematic of active tilting-pad bearing.

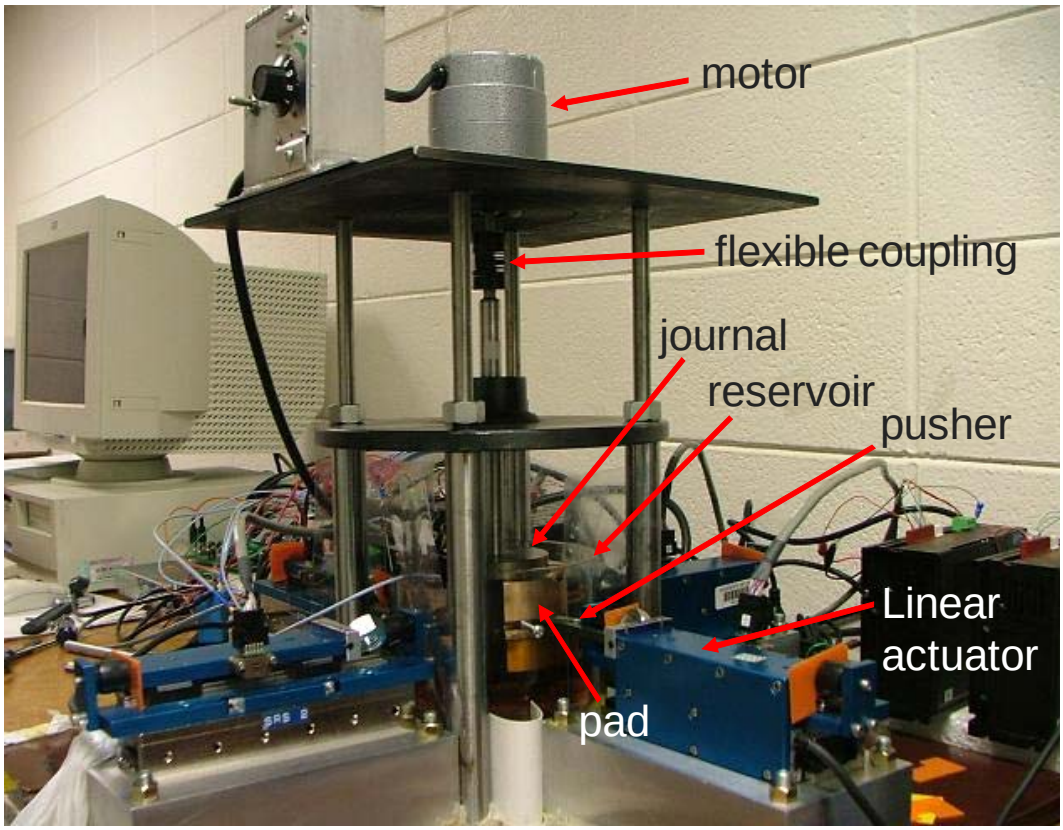

Figure 2.3: The proof-of-concept active tilting-pad bearing test rig.

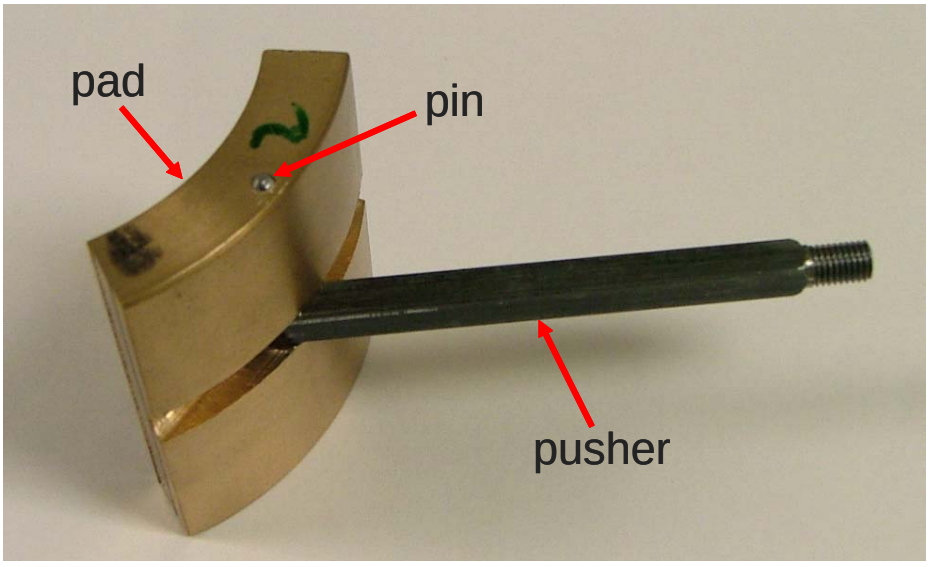

Figure 2.4: Close-up of the pad design.

An AC motor with adjustable speed provided the actuation for the rotor spin, while each pusher is connected to the shaft of a linear actuator system. Each linear actuator system, which was custom designed by H2W Technologies, includes a 3-phase brushless DC linear motor, an optical encoder, and a power amplifier. The bandwidth of the actuation system is 1.5 kHz. An optical encoder with the bandwidth of 100 kHz (resolution ~ 500 CPR), mounted on the linear motor, measured the pad position. The position of the journal center was measured using two Bentley Nevada 3300 Proximity Transducer Systems, located perpendicular to each other. The linear operating range of the probe is 0.254 mm to 2.28 mm from the target. The probe has a static sensitivity of 0.032 mm/V and resolution of 0.32 μm. The output voltage of the displacement probe was applied to an A/D converter. The probes were set so that the maximum and minimum gaps between the rotor and the probe were within the probe's linear range. During the experimental runs, the pads were completely submerged in oil, while the journal was only partially submerged to provide a reflective surface for the probes. The necessary velocity signals were obtained by numerically differentiating the displacement measurements online and then low-pass filtering the resulting signals. The Quanser PCI-MultiQ I/O board was used for data acquisition. Quanser's WinCon system served as the computational engine for: a) coding and running of the control algorithms, b) data transfer between sensors, power amplifiers, and control system, and c) monitoring of the experimental runs. The block diagram of the experimental setup is depicted in Figure 2.5. The test rig parameters are given in Table 2.1. More details about the test rig construction can be found in [4].

2.4 Model Verification

In this section, we verify the dynamic model presented in Section 2.1 through a combination of computational and experimental studies. The two aspects that we will justify are the decoupled nature of the dynamic model and the structure of the hydrodynamic force model in (2.3).

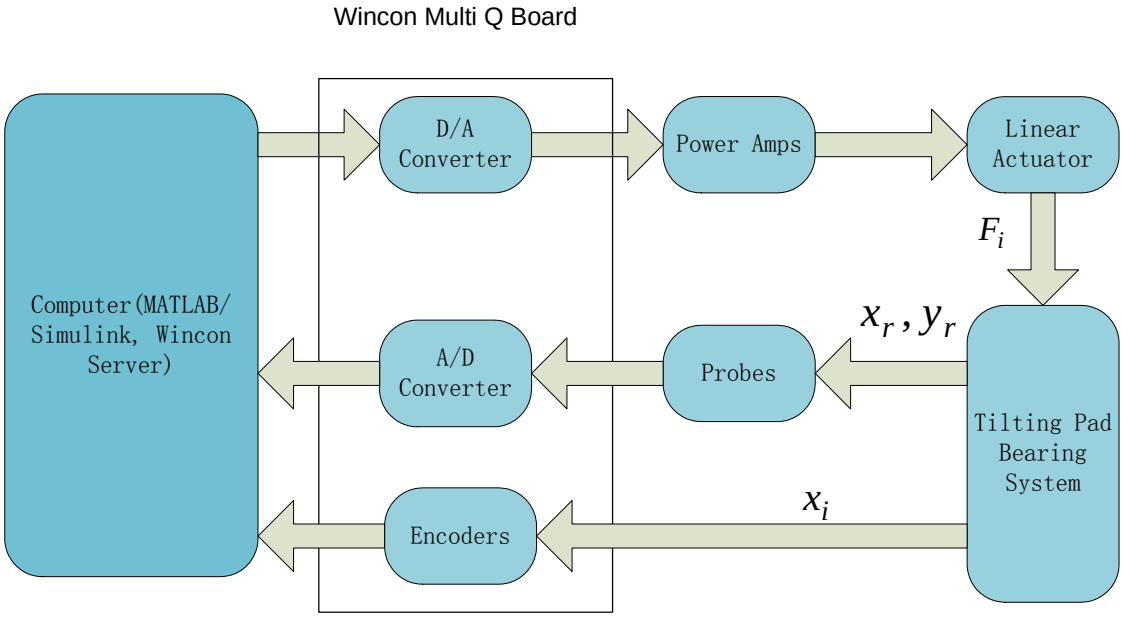

Figure 2.5: Block diagram of the experimental setup.

Table 2.1: Parameters of the Tilting-Pad Bearing Test Rig

Rotor mass (m_r)	3.45 kg
i-th pad mass (m_i)	0.45 kg
i-th pad inertia	1.95×10^{-3} kg $\cdot$ m^2
Pad arc	60°
Pad radius of curvature (R_p)	41 mm
Journal radius (r)	40 mm
Pad length ($L = 2r$)	80 mm
Nominal clearance ($c = R_p - r$)	1 mm
Housing radius	69.85 mm
Rotor speed (ω)	250 rpm (4.167 Hz)
Oil viscosity (5W-20)	0.07 Pa·s

2.4.1 Dynamic Decoupling

We conducted a simple experiment on the test rig to check the assumption that the bearing dynamics are decoupled along the x and y axes. The experiment consisted of manually moving one pad along one of the axes and comparing the rotor displacement along each axis, while the rotor was spinning. The experiment was ran for different rotor speeds with similar results. The results shown in Figure 2.6 are representative of our observations. Figure 2.6a (resp., Figure 2.6c) shows the rotor displacement along both axes when the pad force was applied along the x axis (resp., y axis), while Figure 2.6b (resp., Figure 2.6d) shows the zoomed view of the cross-coupling displacement, i.e., y_r (resp., x_r). The experiment indicates that the cross-coupling displacement is significantly smaller than the displacement along the force axis (viz., 10^2 to 10^3 times smaller). Therefore, we can justify the use of a decoupled dynamic model of the hydrodynamic force between the journal and the pad.

2.4.2 Hydrodynamic Force

The structure of (2.3) is motivated by simulations of the tilting-pad bearing using the numerically-calculated hydrodynamic force (see Section 2.2). Two simulations were conducted to obtain an analytic equation for the hydrodynamic force — one for determining the damping effects, and one for determining the stiffness effects. In both simulations, the rotor angular speed ω was set to 250 rpm. In the stiffness simulation, the rotor position was fixed at the origin ($x_r \equiv 0$), while one pad was radially displaced with zero velocity and a constant tilt angle ($x_1 = [40.5, 42]$ mm, $\dot{x}_1 \equiv 0$, and $\alpha_1 \equiv 0.15^\circ$ where α_i is the tilt angle of the i-th pad). Figure 2.7a shows the resulting stiffness force on the rotor versus $x_1 - x_r$. The plot indicates the stiffness is *always* repellent with the force decreasing as the rotor and pad move apart. Further, the force can be approximated well with a function having the form $f_s(z) = \lambda / (z \pm \sigma)^3$.

In the damping simulation, the rotor position was fixed at the origin, and the pad displacement and instantaneous velocity were independently varied while at a constant tilt angle ($x_r \equiv 0$,

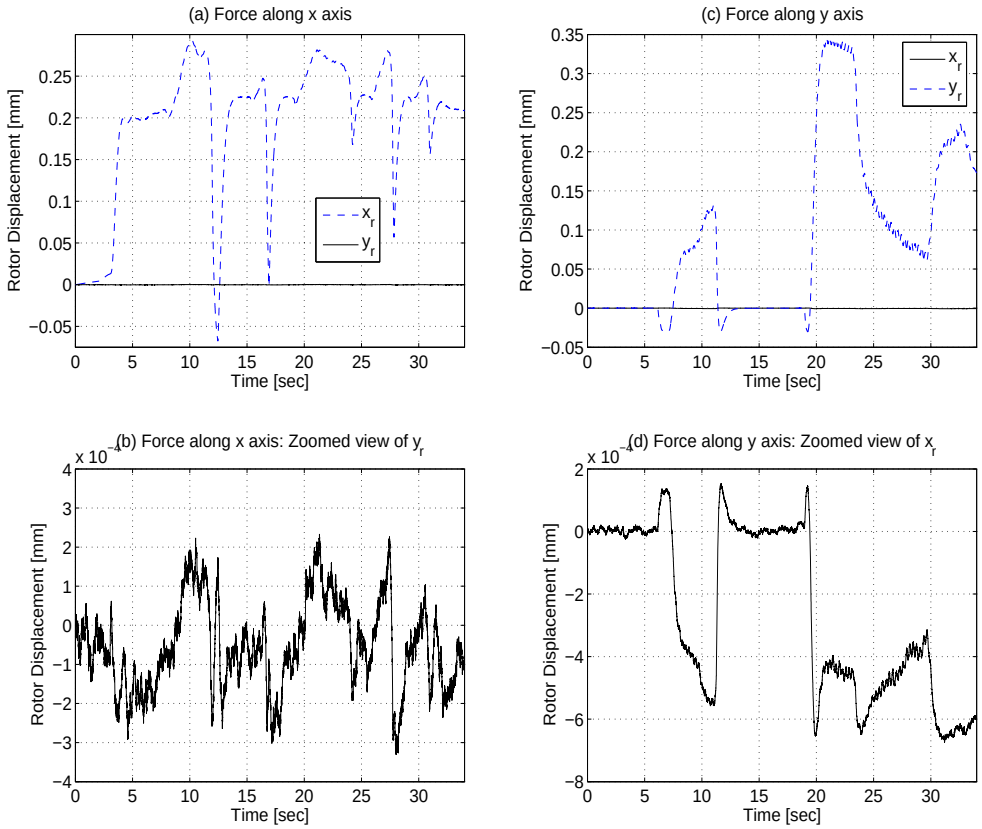

Figure 2.6: Experimental results showing virtual decoupling along the axes of motion.

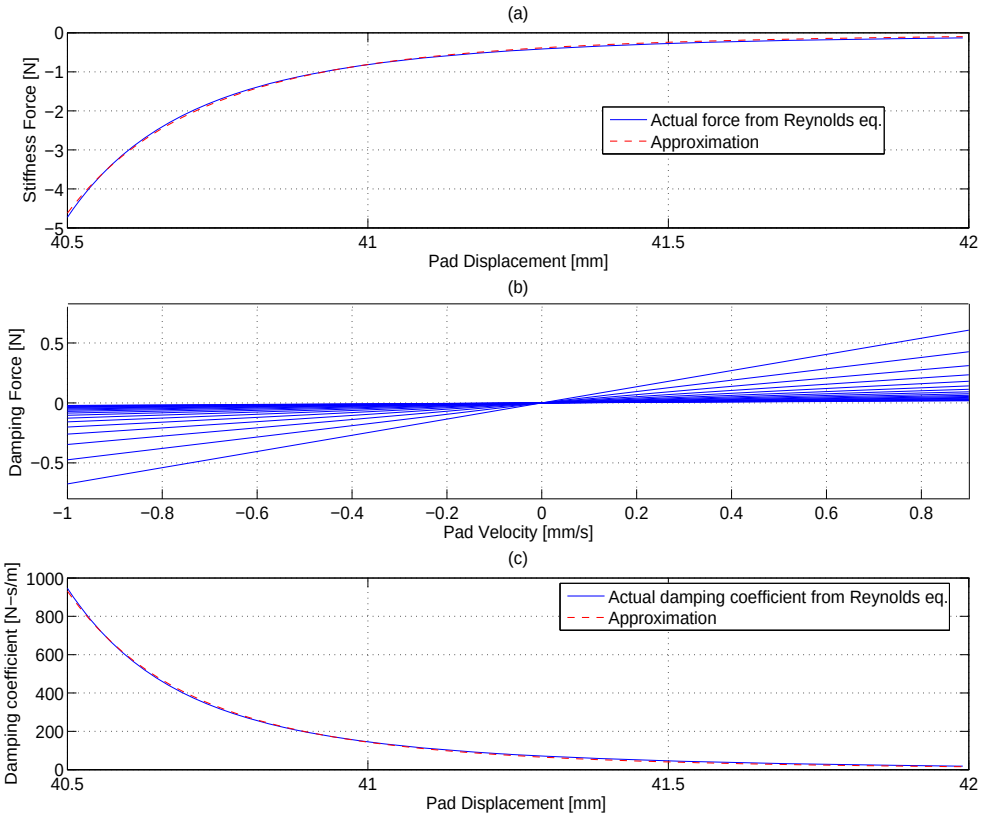

Figure 2.7: Hydrodynamic stiffness and damping force from Reynolds equation.

$x_1 = [40.5, 42]$ mm, $\dot{x}_1 = [-1, 0.9]$ mm/s, and $\alpha_1 \equiv 0.15°$)[1]. Figure 2.7b shows the damping force on the rotor versus $\dot{x}_1 - \dot{x}_r$ for different values of $x_1 - x_r$. The plot indicates the damping force is linear with respect to velocity, but the damping coefficient is dependent on displacement; i.e., $f_d(z) = b(z)\dot{z}$. To investigate the displacement dependency, Figure 2.7c shows the damping coefficient versus $x_1 - x_r$, indicating that the coefficient decreases as the rotor and pad move apart. The coefficient can be approximated well with the function $b(z) = \lambda / (z \pm \sigma)^3$.

The parameters a_i, b_i in (2.3) are dependent on various bearing parameters, including the rotor angular speed, oil viscosity, rotor radius, pad tilt angles, pad length, and pad radius of curvature. The rotor speed, viscosity, and pad tilt angles are the most susceptible to variations and/or uncertainties. Although the pad tilt angles vary in time, their variation is typically very small ($< 1°$). More important, if the pad tilt angles were explicitly included in the control design, their measurements would be required, which would add to the cost of the active bearing. Therefore, we opted to treat the pad tilt angles as constants for control design purposes. Oil viscosity decreases as the oil temperature rises; however, an oil recirculation system is typically used to cool the lubricant and keep the temperature variation to a minimum. Finally, in most rotating machines, the rotor speed is kept constant by the motor controller. Figure 2.8 shows that the parameter a_i is linear in ω and μ, while the parameter b_i is linear in μ and but nonlinear in ω. Note that the nonlinearity in ω is relatively mild since b_i increases linearly with ω up to $\omega \approx 185$ rpm, after which it decreases in a slow exponential-like rate. Thus, the parameters a_i, b_i are not too sensitive to variations in the rotor speed and oil viscosity.

Based on the bearing parameters in Table 2.1, curve-fitting yielded the following values for the parameters in (2.3): $a_i = 4.7242 \times 10^{-10}$ kg·m^4/s^2 and $b_i = 3.1074 \times 10^{-7}$ kg·m^3/s. Further, the parameter σ in the denominator of above approximations functions, $f_s(z)$ and $b(z)$,

[1] To obtain the pure damping force, the stiffness component corresponding to the nonzero value of $x_1 - x_r$ was subtracted from the total hydrdynamic force.

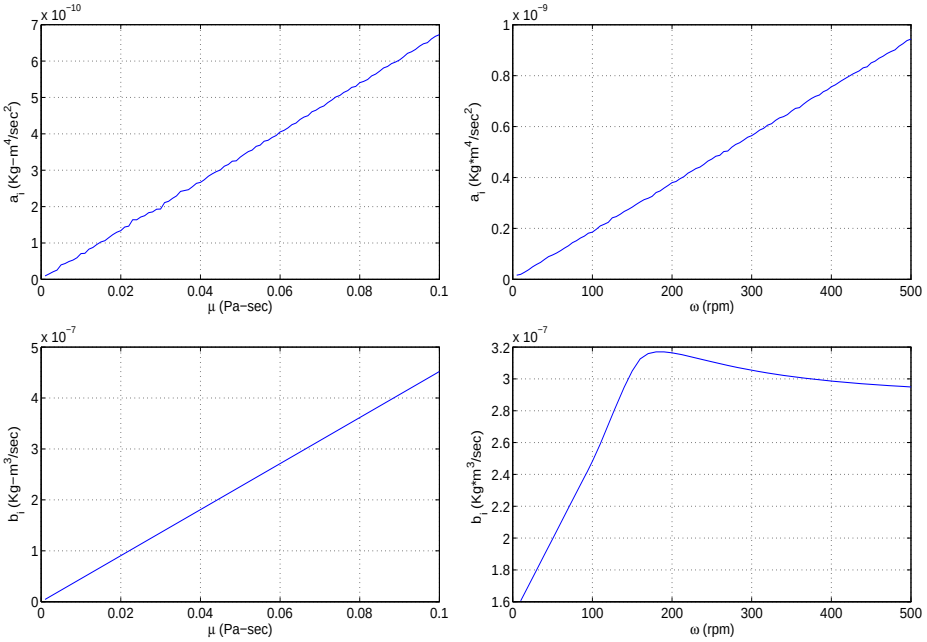

Figure 2.8: Dependency of model parameters a_i and b_i on rotor speed and oil viscosity.

was determined to be $\sigma = 0.0399$ m. It is not a coincidence that this value is approximately the journal radius r (see Table 2.1) since the analytical expression for the hydrodynamic force in simpler, squeeze film bearings often contains a term of the form $1/h^3$ [8]. (Recall that $\left|x_r - x_i + (-1)^{i+1} r\right|$ is the film thickness between the journal and the i-th pad.) Note that the curve-fitting program can be easily and quickly rerun for different parameter sets to yield the corresponding values for a_i and b_i.

2.5 Model-Based Controller

We formulate a model-based nonlinear control law for the dynamics given by (2.1) and (2.3).

2.5.1 Nonlinear Control Law Design

The feedback design that follows is based on the backstepping method [10]. We rewrite (2.1a) in terms of the new variable

$$s = \dot{x}_r + \alpha x_r, \quad \alpha > 0 \tag{2.4}$$

to obtain

$$m_r\dot{s} = (-1)^i \sum_{i=1}^{2} \beta_i(b_i)\,\dot{x}_r - \sum_{i=1}^{2} \beta_i(a_i) + m_r\alpha\dot{x}_r + \sum_{i=1}^{2} (-1)^{i+1}\,\beta_i(b_i)\,v_i + \sum_{i=1}^{2} (-1)^{i+1}\,\beta_i(b_i)\,\eta_i \tag{2.5}$$

where v_i, $i = 1, 2$ denote virtual control inputs,

$$\beta_i(\lambda_i) = \frac{\lambda_i}{\left(x_r - x_i + (-1)^{i+1} r\right)^3}, \quad \forall \lambda_i > 0, \tag{2.6}$$

and

$$\eta_i = \dot{x}_i - v_i. \tag{2.7}$$

Based on (2.5), we design v_i as

$$v_i = \dot{x}_r + (-1)^i \beta_i^{-1}(b_i)\left[k_{si}s - \beta_i(a_i) + \frac{m_r\alpha\dot{x}_r}{2}\right], \quad k_{si} > 0. \tag{2.8}$$

We now turn our attention to the dynamics of the variable η_i. After differentiating (2.7, we obtain

$$\begin{aligned} m_i\dot{\eta}_i \;=\;& (-1)^i \beta_i(b_i)(\dot{x}_i - \dot{x}_r) + \beta_i(a_i) + F_i \\ & - \left[1 + (-1)^i \beta_i^{-1}(b_i)\left(k_{si} + \frac{m_r\alpha}{2}\right)\right]\frac{m_i}{m_r}\sum_{i=1}^{2}\left[(-1)^{i+1}\beta_i(b_i)(\dot{x}_i - \dot{x}_r) - \beta_i(a_i)\right] \\ & + (-1)^{i+1} m_i\beta_i^{-2}(b_i)\left(\frac{\partial\beta_i(b_i)}{\partial x_i}\dot{x}_i + \frac{\partial\beta_i(b_i)}{\partial x_r}\dot{x}_r\right)\left[k_{si}s - \beta_i(a_i) + \frac{m_r\alpha\dot{x}_r}{2}\right] \\ & + (-1)^i m_i\beta_i^{-1}(b_i)\left[k_{si}\alpha\dot{x}_r - \frac{\partial\beta_i(a_i)}{\partial x_i}\dot{x}_i - \frac{\partial\beta_i(a_i)}{\partial x_r}\dot{x}_r\right]. \end{aligned} \tag{2.9}$$

The i-th control input force is designed as

$$F_i = -k_{pi}\eta_i - W_i(x_i, \dot{x}_i, x_r, \dot{x}_r) - \beta_i(b_i)\,s, \quad k_{pi} > 0 \tag{2.10}$$

where the nonlinearity W_i is defined as

$$\begin{aligned} W_i \;=\;& (-1)^i \beta_i(b_i)(\dot{x}_i - \dot{x}_r) + \beta_i(a_i) \\ & - \left[1 + (-1)^i \beta_i^{-1}(b_i)\left(k_{si} + \frac{m_r\alpha}{2}\right)\right]\frac{m_i}{m_r}\sum_{i=1}^{2}\left[(-1)^{i+1}\beta_i(b_i)(\dot{x}_i - \dot{x}_r) - \beta_i(a_i)\right] \\ & + (-1)^{i+1} m_i\beta_i^{-2}(b_i)\left(\frac{\partial\beta_i(b_i)}{\partial x_i}\dot{x}_i + \frac{\partial\beta_i(b_i)}{\partial x_r}\dot{x}_r\right)\left[k_{si}s - \beta_i(a_i) + \frac{m_r\alpha\dot{x}_r}{2}\right] \\ & + (-1)^i m_i\beta_i^{-1}(b_i)\left[k_{si}\alpha\dot{x}_r - \frac{\partial\beta_i(a_i)}{\partial x_i}\dot{x}_i - \frac{\partial\beta_i(a_i)}{\partial x_r}\dot{x}_r\right]. \end{aligned} \tag{2.11}$$

2.5.2 Stability Analysis

Select the following Lyapunov function candidate

$$V = \frac{1}{2} m_r s^2 + \frac{1}{2} \sum_{i=1}^{2} m_i \eta_i^2. \tag{2.12}$$

After differentiating (2.12) along (2.5) and (2.9) in closed loop with (2.8) and (2.10), we obtain

$$\dot{V} = -\sum_{i=1}^{2} k_{si} s^2 - \sum_{i=1}^{2} k_{pi} \eta_i^2. \tag{2.13}$$

From (2.12) and (2.13), we can show that $s(t), \eta_i(t) \to 0$ as $t \to \infty$ exponentially fast with convergence rate proportional to min(k_{si}, k_{pi}), $i = 1, 2$. It then follows from (2.4) that $x_r(t), \dot{x}_r(t) \to 0$ as $t \to \infty$ exponentially fast. The boundedness of all other closed-loop signals is straightforward to establish.

2.6 Experimental Results

Here, we describe a proof-of-concept experiment of the proposed control system for active tilting-pad bearings. The main goal of the experiment is to demonstrate that the active control can improve the performance of the tilting-pad bearing system relative to its traditional, passive mode of operation. A secondary goal is to compare the proposed model-based nonlinear controller, given by (2.8) and (2.10), with the following linear PID controller

$$F_i = -k_{pi} \eta_i, \quad v_i = \dot{x}_r - k_{si} s - k_{Ii} \int s(t) \mathrm{d}t, \quad k_{Ii} > 0. \tag{2.14}$$

In all experimental runs, the following procedure was adopted. The experiment was initiated by turning on the rotor motor at 250 rpm with the tilting-pad bearing operating in its traditional, passive mode of operation. This was done by introducing (four) stoppers to fix each pad pusher in the radial direction. At $0 < t < 5$ seconds, the stoppers were removed, causing the pads to translate because of the hydrodynamic pressure, but the controller was not yet turned on (i.e., a "semi-passive" bearing). At $t = 10$ seconds, the controller was turned on so the bearing would become active. Control gains were tuned for the best regulation performance possible, resulting in

the following values for the gains[2]. Model-based control: $\alpha_{12} = 200$, $\alpha_{34} = 100$, $k_{pi} = k_{si} = 10$ ($i = 1, \ldots, 4$); PID control: same gains as the model-based control and $k_{Ii} = 100$ ($i = 1, \ldots, 4$). The experiment was run several times for each controller with similar results. Therefore, the results shown in the following figures are representative of our observations.

Figure 2.9 depicts the position of the journal center $(x_r(t), y_r(t))$ under the model-based nonlinear controller. First, the figure shows that the passive bearing nor the semi-passive bearing are capable of running the journal concentrically in the clearance. However, the journal position is successfully regulated to zero once the controller is activated. The control forces in the x direction of the model-based nonlinear controller for $10 \leq t \leq 15$ seconds are shown in Figure 2.10. The y-direction forces had a similar profile and thus are not presented. The results for the linear PID controller are shown in Figures 2.11 and 2.12. The PID controller also regulates the journal position to zero. However, the PID control forces exhibit a steady-state bias of approximately 2 N, which does not occur with the model-based control. To quantify the energy expended by each controller, we calculated the following quantity for each one,

$$E_c = \int_{10}^{15} \sum_{i=1}^{4} F_i^2(t) \mathrm{d}t.$$

The results are the following: $E_c = 30.3$ N^2·s for the model-based control, and $E_c = 93.2$ N^2·s for the PID control. This indicates that the PID controller required significantly more energy than the model-based controller to yield a comparable regulation performance. We note that the small steady-state oscillations seen in all the displacement and force plots are likely due to rotor unbalance since their frequency is approximately equal to the rotor speed.

Remark 1 Mathematical models never provide a perfect representation of the plant dynamics. In the case of the tilting-pad bearing system, mismatch between the model (2.1)-(2.3) and the actual

[2] From now on, subscripts 1 and 2 denote parameters/variables in the x direction, while subscripts 3 and 4 denote parameters/variables in the y direction in accordance to Figure 1.1. Also, subscript 12 (resp., 34) indicates an x-direction (resp., y-direction) parameter.

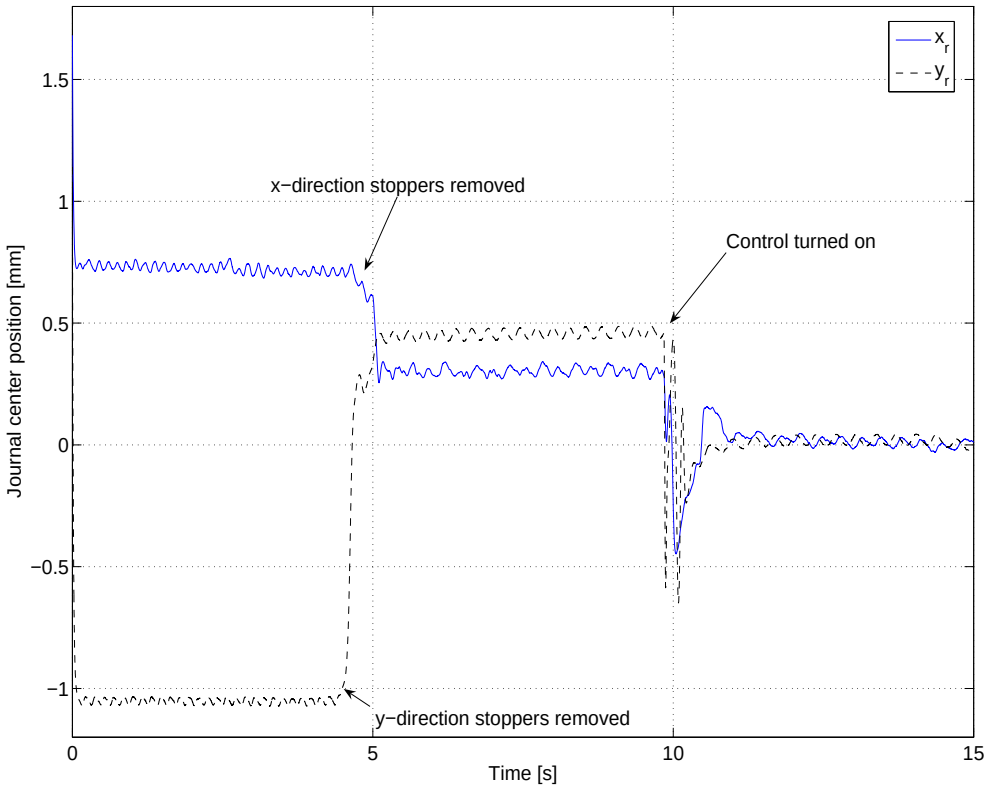

Figure 2.9: Experimental results for model-based nonlinear controller: position of journal center $(x_r(t), y_r(t))$.

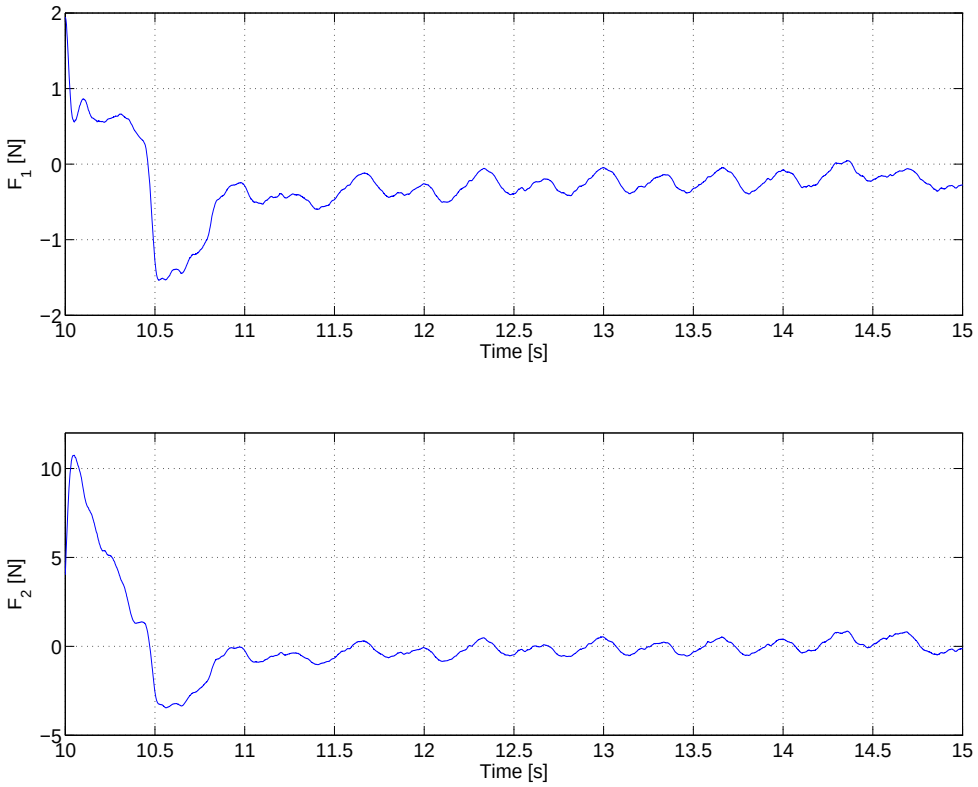

Figure 2.10: Experimental results for model-based nonlinear controller: control forces in x-direction $F_1(t)$ and $F_2(t)$.

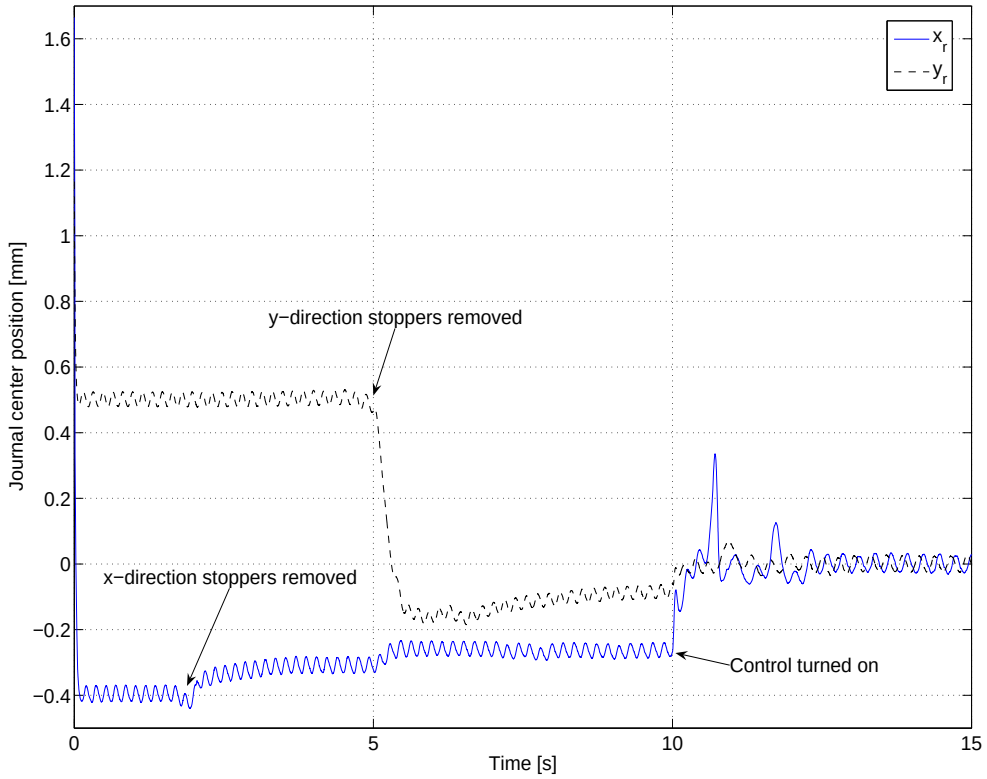

Figure 2.11: Experimental results for linear PID controller: position of journal center $(x_r(t), y_r(t))$.

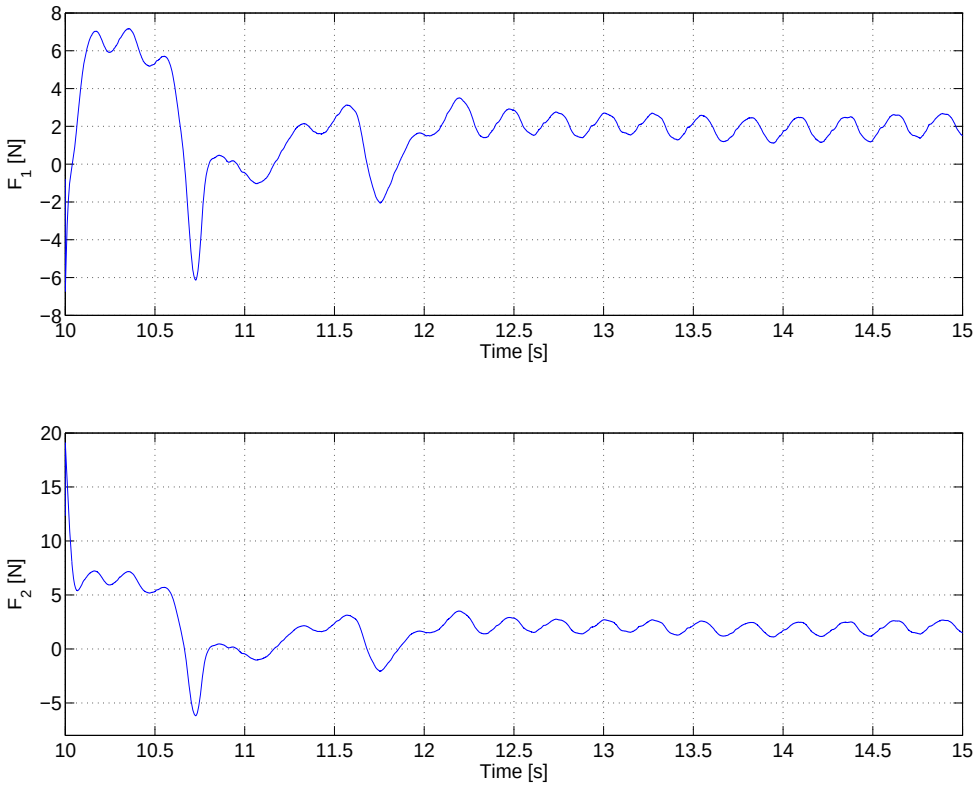

Figure 2.12: Experimental results for linear PID controller: control forces in x-direction $F_1(t)$ and $F_2(t)$.

dynamics can occur due to, for example, shaft flexibility and misalignment, rotor unbalance, variation in the fluid viscosity, sensor noise, and actuator bandwidth and saturation. Note that adaptive and robust versions of the proposed nonlinear control strategy could be designed to compensate for certain modeling uncertainties. However, the experimental results have demonstrated that the proposed model-based control is sufficiently robust to plant uncertainties. That is, if we disregard the unbalanced-induced steady-state vibrations in Figure 2.9, the proposed control would have likely regulated the journal to the bearing center. In addition, the model-based controller could be redesigned to compensate for rotor unbalance. This was not done here since our goal was to provide a *relative performance comparison* with the passive bearing and the PID-type controller.

Chapter 3 Tilting-Pad Bearings with Active Pad Tilt

In this chapter, we propose a new type of active tilting-pad bearing. Specifically, we actuate the *tilt angle* of each pad and use the pad angular velocities as control inputs.

3.1 Bearing System Model

3.1.1 General Equations of Motion

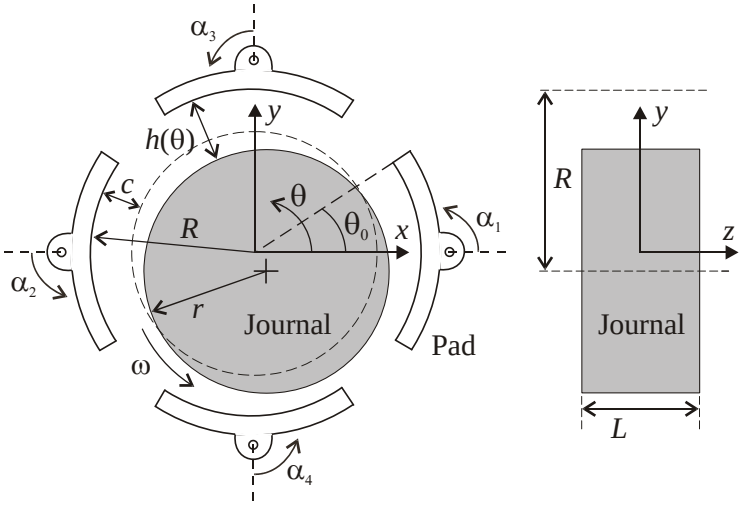

Figure 3.1: The tilting-pad bearing system.

Consider the tilting-pad bearing system in Figure 3.1. The *coupled* equations of motion are

$$m\ddot{q} = F_h(q, \dot{q}, \alpha, \dot{\alpha}, q_p, \dot{q}_p) + W \tag{3.1}$$

where m is the constant journal mass, $q = (x, y)$ is the position of the journal center, $\alpha \in \mathbb{R}^4$ is the vector of pad title angles, $q_p \in \mathbb{R}^4$ represents the vector of pad radial positions, $F \in \mathbb{R}^2$ denotes the total hydrodynamic force the fluid film applies on the journal, and $W \in \mathbb{R}^2$ is the constant external load. Note that when the tilting-pad bearing has a zero preload factor [2], $q_p = (R, -R, R, -R)$ where $R > 0$ is the radius of circle formed by the pads with $\alpha = 0$. Further, let $c = R - r$ be the nominal clearance (i.e., nominal fluid film thickness), L be the bearing axial length, and $\mathcal{S}_i = [(i-1)\,\pi/2 - \theta_0, (i-1)\,\pi/2 + \theta_0]$, $i = 1, 2, 3, 4$ be the arc of the ith pad in terms of the θ coordinate where $\theta_0 > 0$.

Recall that one of the key issues in (3.1) is the model for the hydrodynamic force. Under the assumption of an infinitely short bearing (i.e., $L/(2r) < 0.5$), we will derive an expression for F from the one-dimensional Reynolds equation [8]

$$\frac{\partial}{\partial z}\left(h^3\frac{\partial p}{\partial z}\right) = 6\mu\omega\frac{\partial h}{\partial \theta} + 12\mu\frac{\partial h}{\partial t}. \tag{3.2}$$

Specifically, by solving (3.2), we can obtain an analytical solution for the pressure field along each pad arc. Then, solving the following integrals along the pad surface area yield the hydrodynamic forces along the x and y directions due to each pad:

$$F_i = \begin{bmatrix} F_{xi} \\ F_{yi} \end{bmatrix} = r\int_{-\frac{L}{2}}^{\frac{L}{2}}\int_{\underline{\theta}_i}^{\overline{\theta}_i} p_i \begin{bmatrix} \cos\theta \\ \sin\theta \end{bmatrix} \mathrm{d}\theta\mathrm{d}z,\ i = 1,2,3,4 \tag{3.3}$$

where F_i, p_i denote the force and pressure from the ith pad, respectively and $\mathcal{N}_i = \left[\underline{\theta}_i, \overline{\theta}_i\right] \subseteq \mathcal{S}_i$, $0 < \underline{\theta}_i \leq \overline{\theta}_i$ denotes the portion of the ith pad arc where the pressure is nonnegative.

3.1.2 Control Inputs

To transform the tilting-pad bearing into an active system, $\dot{\alpha}$ is proposed to be utilized as the control input to (3.1), as opposed to the more common choice of $\dot{q}_p$ (see Chapter 2). This new active approach is primarily based on the following two observations: a) the wedge action has more pressure-generating capacity (i.e., control authority) than the squeeze action [8, 9], and b) the pad tilting (resp., radial) motion has a direct effect on the wedge (resp., squeeze) action. To illustrate this, consider the tilting-pad bearing system with the parameter values in Table 3.1 and $q \equiv 0$. We will compare the static pressure field generated by Pad 1 when: (i) it is displaced in the $-x$ direction while $\alpha_1 \equiv 0$ (pure normal squeeze), and (ii) it is tilted in the $+\alpha$ direction while $q_{p1} \equiv R$ (no preloading). For case (i), let $d = R - q_{p1}$; thus, the maximum linear displacement range for the pad (i.e., before it comes in contact with the journal) is $d \in [0, d_{\max}] = [0, c = 0.1]$ mm. For case (ii), the maximum angular displacement range for the pad is $\alpha_1 \in [0, \alpha_{\max}] = [0, 4.89]$ mrad. See Figure 3.2 for an illustration of the maximum ranges of pad translation and angular displacement.

Table 3.1: Bearing System Parameters

m	3 kg
r	40.9 mm
R	41 mm
c	0.1 mm
L	20.45 mm ($= r/2$)
ω	1000 rpm
μ	0.027 kg/(m·sec)
θ_0	$\pi/6$ rad

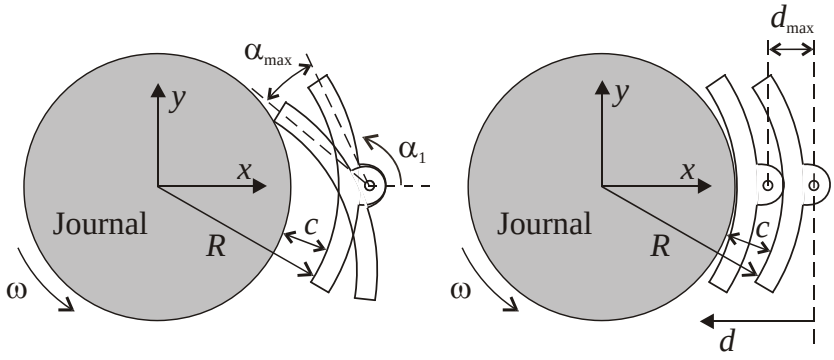

Figure 3.2: Maximum pad displacement ranges.

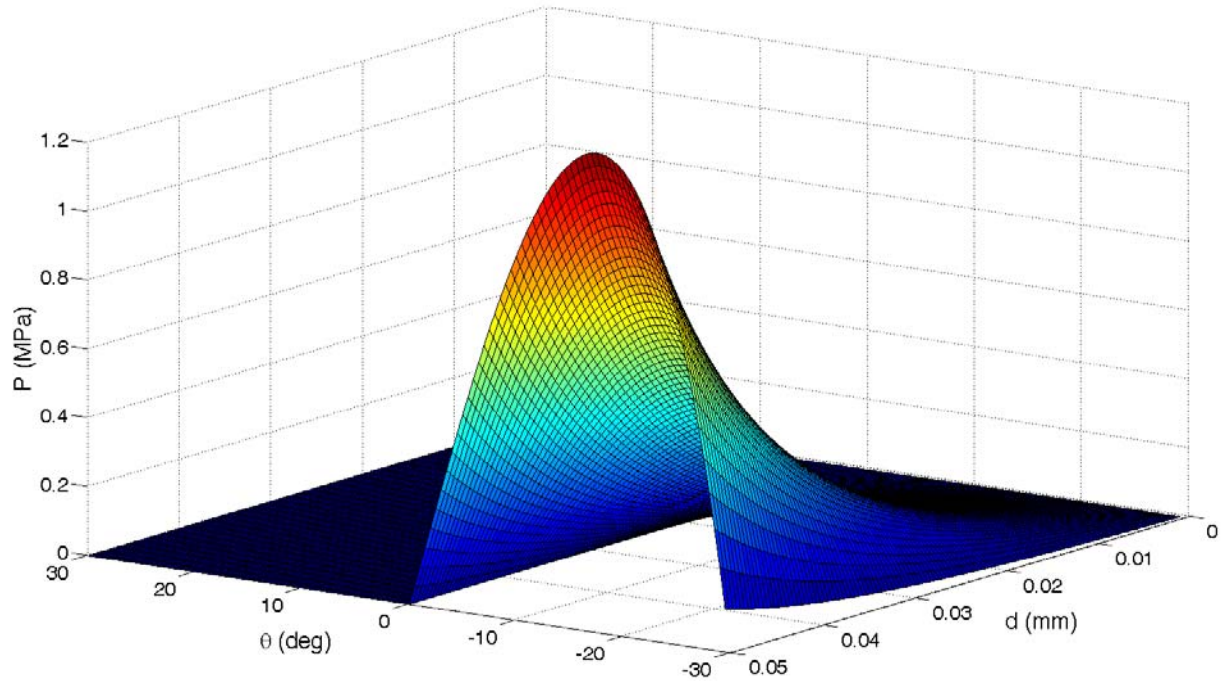

Figure 3.3: Pressure along pad arc as a function of pad radial position.

Figures 3.3 and 3.4 show the static pressure field for the two cases when the pad was displaced by 50% of the maximum ranges. To facilitate the comparison, the angular displacement in case (ii) was multiplied by the radius of curvature of the pad, R, to approximate the linear displacement of the pad's upper edge. The pressure field was determined by numerically solving (3.2). The zero pressure at $\theta \geq 0^{\circ}$ in Figure 3.3 accounts for the divergent oil film in the upper half of the pad which develops during the squeeze motion. We can see from Figures 3.3 and 3.4 that slight variations in the pad tilt angle can generate larger peak pressures than variations in the pad radial position. We also calculated the volume under each surface (V_p) to serve as a measure of the overall pressure-generating capacity of each scheme. We determined that $V_p = 0.6287$ Pa-m for case (i) and $V_p = 10.59$ Pa-m for case (ii). These results suggest that the active 'wedge' approach yields better controllability properties than the active 'squeeze' approach.

Finally, note that with the choice of $\dot{\alpha}$ as the control input and the pads radial position fixed at $\pm R$, the *variable* dependency of the hydrodynamic force in (3.1) is reduced to $F(q, \dot{q}, \alpha, \dot{\alpha})$.

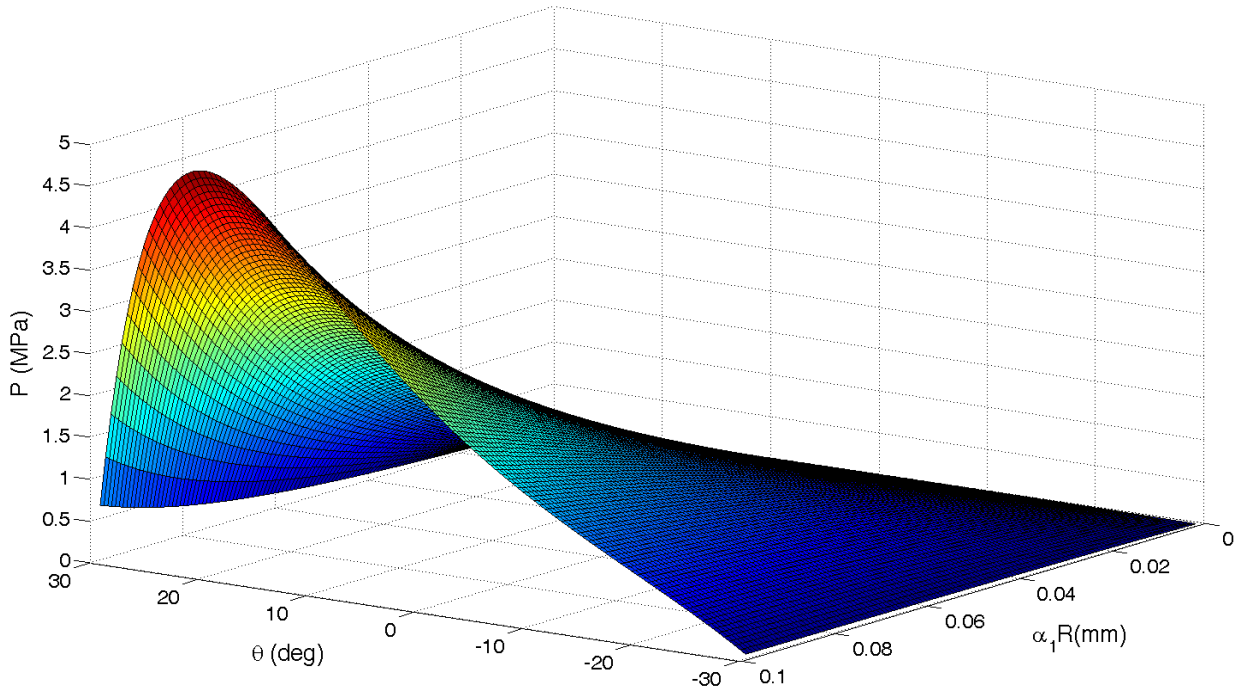

Figure 3.4: Pressure along pad arc as a function of pad tilt angle.

3.1.3 Hydrodynamic Force Model

We now present the proposed model for the hydrodynamic force. To this end, the solution of the reduced Reynolds equation (3.2) for the ith pad is given by [12]

$$p_i(q, \dot{q}, \alpha_i, \dot{\alpha}_i, \theta, z) = \frac{\upsilon_i \sin\theta - \sigma_i \cos\theta}{h_i^3} \left(\frac{4z^2}{L^2} - 1 \right) \tag{3.4}$$

where $-L/2 \leq z \leq L/2$ and

$$\upsilon_i = \frac{3L^2\mu}{4} \left(\omega x_{pi} - 2\dot{y}_{pi} \right), \qquad \sigma_i = \frac{3L^2\mu}{4} \left(\omega y_{pi} + 2\dot{x}_{pi} \right) \tag{3.5}$$

$$x_{pi} = x - r\alpha_i \sin\left(i-1\right)\frac{\pi}{2}, \qquad y_{pi} = y + r\alpha_i \cos\left(i-1\right)\frac{\pi}{2} \tag{3.6}$$

$$h_i = c - x_{pi}\cos\theta - y_{pi}\sin\theta \tag{3.7}$$

To calculate the integrals in (3.3), we follow the procedure of [12]. First, after substituting (3.4) into (3.3) and integrating along z, we obtain

$$F_i = -\frac{2Lr}{3} \int_{\underline{\theta}_i}^{\overline{\theta}_i} \frac{\upsilon_i \sin\theta - \sigma_i \cos\theta}{h_i^3} \begin{bmatrix} \cos\theta \\ \sin\theta \end{bmatrix} \mathrm{d}\theta. \tag{3.8}$$

Let $V_i = h_i^{-1}$; thus,

$$\frac{\partial^2 V_i}{\partial x_{pi}^2} = \frac{2\cos^2\theta}{h_i^3}, \qquad \frac{\partial^2 V_i}{\partial y_{pi}^2} = \frac{2\sin^2\theta}{h_i^3}, \qquad \frac{\partial^2 V_i}{\partial x_{pi}\partial y_{pi}} = \frac{2\sin\theta\cos\theta}{h_i^3}, \tag{3.9}$$

so (3.8) becomes

$$F_i = -\frac{Lr}{3}\int_{\underline{\theta}_i}^{\overline{\theta}_i} \begin{bmatrix} \frac{\partial^2 V_i}{\partial x_{pi}\partial y_{pi}} & -\frac{\partial^2 V_i}{\partial x_{pi}^2} \\ \frac{\partial^2 V_i}{\partial y_{pi}^2} & -\frac{\partial^2 V_i}{\partial x_{pi}\partial y_{pi}} \end{bmatrix} \begin{bmatrix} \upsilon_i \\ \sigma_i \end{bmatrix} \mathrm{d}\theta. \tag{3.10}$$

Next, let

$$\Lambda_i = \int V_i \mathrm{d}\theta, \quad A_i = \frac{\partial^2 \Lambda_i}{\partial x_{pi}^2}, \quad B_i = \frac{\partial^2 \Lambda_i}{\partial x_{pi}\partial y_{pi}}, \quad C_i = \frac{\partial^2 \Lambda_i}{\partial y_{pi}^2} \tag{3.11}$$

and

$$\begin{gathered} d_{1i} = x_{pi}^2 + y_{pi}^2 - c^2, \qquad d_{2i} = \tan\frac{\theta}{2},\ \theta \in \mathcal{N}_i, \qquad d_{3i} = y_{pi} - (c + x_{pi})\, d_2, \\ d_{4i} = \tanh^{-1}\left(\frac{d_{3_i}}{\sqrt{d_{1i}}}\right); \end{gathered} \tag{3.12}$$

thus

$$\Lambda_i = \frac{2d_{4i}}{\sqrt{d_{1i}}}, \tag{3.13}$$

$$\begin{aligned} A_i \;=\; & -\frac{2\left(d_{1i} - 3x_{pi}^2\right) d_{4i}}{d_{1i}^{5/2}} + \frac{2d_{3i}\left(d_{3i}^2 + 2d_{2i}d_{3i}x_{pi} + 3\kappa_i^2\right)}{d_{1i}\left(d_{1i} - d_{3i}^2\right)^2} + \frac{-6d_{3i}^3 x_{pi}^2 + 4d_{1i}d_{3i}x_{pi}\left(x_{pi} - d_{2i}d_{3i}\right)}{d_{1i}\left(d_{1i} - d_{3i}^2\right)^2} \\ & + \frac{d_{1i}^2\left[\left(4d_{2i}^2 - 2\right)d_{3i} + 8d_{2i}x_{pi}\right]}{d_{1i}\left(d_{1i} - d_{3i}^2\right)^2}, \end{aligned} \tag{3.14}$$

$$B_i = \frac{6x_{pi}y_{pi}d_{4i}}{d_{1i}^{5/2}} - \frac{4d_{3i}\left(d_{1i}d_{2i} + d_{3i}x_{pi}\right)\left(d_{1i} - d_{3i}y_{pi}\right)}{d_{1i}^2\left(d_{1i} - d_{3i}^2\right)^2} - \frac{4d_{1i}x_{pi} - 4d_{1i}d_{2i}y_{pi} - 10d_{3i}x_{pi}y_{pi}}{d_{1i}^2\left(d_{1i} - d_{3i}^2\right)}, \tag{3.15}$$

and

$$\begin{aligned} C_i \;=\; & -\frac{2\left(d_{1i} - 3y_{pi}^2\right) d_{4i}}{b_1^{5/2}} - \frac{4y_{pi}\left(d_{1i} - d_{3i}y_{pi}\right)}{d_{1i}^2\left(d_{1i} - d_{3i}^2\right)} + \frac{2\left[d_{1i}^2\left(d_{3i} - 2y_{pi}\right) - d_{3i}^3 y_{pi}^2\right]}{d_{1i}^2\left(d_{1i} - d_{3i}^2\right)^2} \\ & + \frac{2d_{1i}d_{3i}\left(d_{3i}^2 - 2d_{3i}y_{pi} + 3y_{pi}^2\right)}{d_{1i}^2\left(d_{1i} - d_{3i}^2\right)^2}. \end{aligned} \tag{3.16}$$

It is not difficult to see that (3.10) can now be written as

$$F_i(q, \dot{q}, \alpha_i, \dot{\alpha}_i) = -\frac{Lr}{3}\begin{bmatrix} B_i & -A_i \\ C_i & -B_i \end{bmatrix}\begin{bmatrix} \upsilon_i \\ \sigma_i \end{bmatrix}\Bigg|_{\underline{\theta}_i}^{\overline{\theta}_i}. \tag{3.17}$$

It follows from (3.17) that the total hydrodynamic force acting on the journal is given by

$$\begin{aligned} F &= \sum_{i=1}^{4} F_i \\ &= -\frac{Lr}{3}\sum_{i=1}^{4}\begin{bmatrix} B_i & -A_i \\ C_i & -B_i \end{bmatrix}\begin{bmatrix} \frac{3L^2\mu}{4}(\omega x_{pi} - 2\dot{y}) \\ \sigma_i \end{bmatrix} - 2r\cos(i-1)\frac{\pi}{2}\begin{bmatrix} B_i \\ C_i \end{bmatrix}\dot{\alpha}_i\Big|_{\underline{\theta}_i}^{\overline{\theta}_i} \end{aligned} \tag{3.18}$$

3.2 Feedback Control Design

3.2.1 Controlled Dynamics

Based on (3.18), the equations of motion (3.1) can be expressed as follows

$$m\ddot{q} = \psi(q,\dot{q},\alpha) + W + G(q,\alpha)u \tag{3.19}$$

where $u = \dot{\alpha}$ is the control input and the nonlinear functions $\psi \in \mathbb{R}^2$ and $G \in \mathbb{R}^{2\times 4}$ are defined as

$$\psi = -\frac{Lr}{3}\sum_{i=1}^{4}\begin{bmatrix} B_i & -A_i \\ C_i & -B_i \end{bmatrix}\begin{bmatrix} \frac{3L^2\mu}{4}(\omega x_{pi} - 2\dot{y}) \\ \sigma_i \end{bmatrix}\Big|_{\underline{\theta}_i}^{\overline{\theta}_i} \tag{3.20}$$

$$G = \frac{2Lr^2}{3}\cos(i-1)\frac{\pi}{2}\begin{bmatrix} B_1 & B_2 & B_3 & B_4 \\ C_1 & C_2 & C_3 & C_4 \end{bmatrix}. \tag{3.21}$$

We consider a horizontal rotor shaft such that $W = (0, -W_0)$ where $W_0 > 0$ denotes the rotor weight. We make the following assumptions regarding the above controlled dynamics.

A1. A fluid film is always present between the journal and pads, i.e., $h_i(q,\alpha_i) > 0$ in (3.7) $\forall q, \alpha_i$, $i = 1,2,3,4$.

A2. The variable α is bounded for all time.

A3. The input matrix G has full row rank for $\forall q, \alpha$.

The above assumptions are physically reasonable for the following reasons. First, in hydrodynamic bearings, the lubricant film is generally thick enough so that the bearing and journal do not come into contact [8]. Second, one can place stoppers on both sides of each pad [18] such that $-\underline{\alpha}_i \le \alpha_i \le \overline{\alpha}_i$ where $\underline{\alpha}_i > \overline{\alpha}_i > 0$. Third, both the direction of the journal angular speed and the presence of a vertical load create an asymmetry in the equilibrium tilt angle of each pad necessary to maintain the journal center at the desired equilibrium point $(q,\dot{q}) = 0$. This asymmetry ensures that, at equilibrium, at least two pad angles will be different (e.g., $\alpha_1 \neq \alpha_2$),

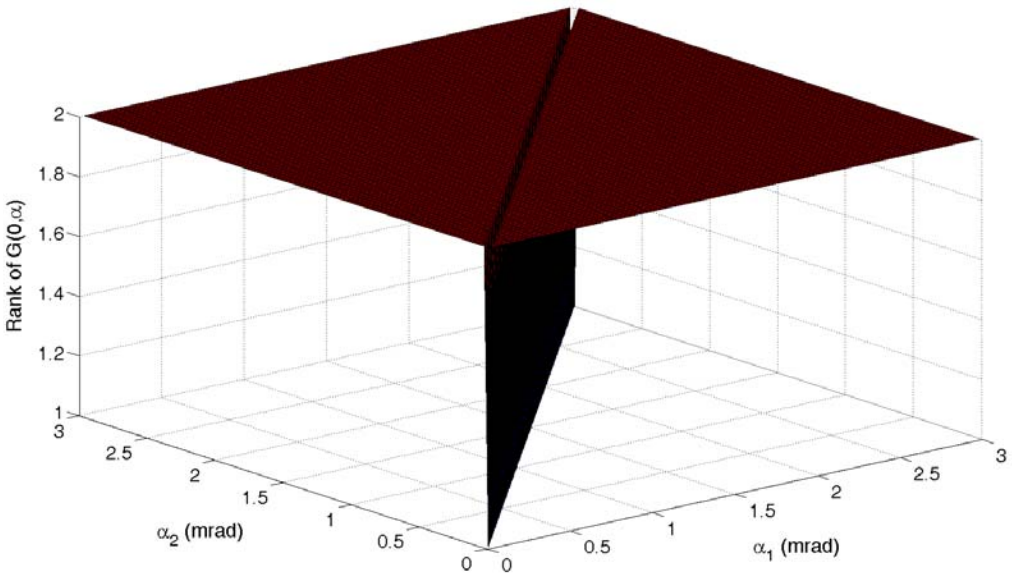

Figure 3.5: Rank of $G(0, \alpha)$ versus α_1 and α_2.

which in turn ensures that two columns of G are linearly independent (e.g., columns 1 and 2 of G are linearly independent) and thus the rank of G is 2. To illustrate this, we calculated the rank of $G(0, \alpha)$ using the first two columns of the matrix. The result is displayed in Figure 3.5 and shows that the only situation where $G(0, \alpha)$ loses its full row rank is when $\alpha_1 = \alpha_2$.

Remark 2 The physical realization of the proposed control input would require an electric motor actuating each pad. We opted to neglect the dynamics of the pad tilt motion in order to focus on the key contribution of this work, viz., the control of the journal dynamics by actively tilting the pads. However, one can easily and rigorously account for the pad tilt dynamics with motor torque input in the control design via the backstepping method [10]. Alternatively, one can in practice implement a "high-gain" velocity feedback loop at the torque level (see subsequent simulation results).

Remark 3 Recall that dynamic model for the active tilting-pad bearing in Chapter 2 was *decoupled* (see Section (2.1)), whereas the dynamic model (3.19) is coupled. The coupled and thus multivariable nature of (3.19) introduces an additional challenge for the design of a model-based control law for this new active bearing.

3.2.2 Control Law

Our control objective is to design a model-based feedback law for u, under the assumption that q, $\dot{q}$, and α are measurable, such that $q(t), \dot{q}(t) \to 0$ as $t \to \infty$. To this end, we rewrite (3.19) in terms of the following variable

$$s = \dot{q} + K_1 q \tag{3.22}$$

where $K_1 \in \mathbb{R}^{2\times 2}$ is constant, symmetric, and positive definite. As a result, we obtain

$$m\dot{s} = \psi(q, \dot{q}, \alpha) + W + G(q, \alpha)u + mK_1\dot{q}. \tag{3.23}$$

From (3.23), we design the control input to be

$$u = G^{+}\left(-\psi - W - mK_1\dot{q} - mK_2 s\right) \tag{3.24}$$

where $G^{+} = G^{T}\left(GG^{T}\right)^{-1}$ is the Moore-Penrose inverse, i.e., $GG^{+} = I_2$ [16], and $K_2 \in \mathbb{R}^{2\times 2}$ is constant, symmetric, and positive definite. This yields the exponentially stable, linear closed-loop system $\dot{s} = -K_2 s$, i.e., $s(t) \to 0$ as $t \to \infty$ exponentially fast. It follows from (3.22) that $\dot{q} = -K_1 q + s$ and therefore $q(t), \dot{q}(t)$ are bounded and $q(t), \dot{q}(t) \to 0$ as $t \to \infty$ (see, e.g., Theorem 2.13 of [17]) with convergence rate dependent on the eigenvalues of K_1 and K_2. Further, due to assumption A1 and the continuity properties of ψ and G, u is bounded for all time.

Remark 4 The limits $\underline{\theta}_i$ and $\overline{\theta}_i$ that are needed to compute ψ and G for (3.24) (see (3.20) and (3.21)) can be determined online from measurements of q, $\dot{q}$, and α by calculating (3.4) at $z = 0$ for different values of $\theta \in \mathcal{S}_i$, and checking the minimum and maximum angles for which $p_i(\theta) \geq 0$. Further, one can avoid the term $\tan \pi/2 = \infty$ in d_{22} (see (3.12)) during the calculation of ψ and G by exploiting the fact that $F_2 = -F_1(-q, -\dot{q}, \alpha_2, \dot{\alpha}_2)$.

3.3 Simulation Results

The proposed active tilting-pad bearing under control of the feedback law in (3.24) was simulated in comparison to the bearing's standard passive operation. When simulating (3.1), (1.1)

and (3.3) were numerically solved to give the "exact" hydrodynamic forces. The details of this numerical calculation can be found in, for example, [4]. We also included the dynamics of the pad tilting motion, which are given by

$$J\ddot{\alpha} + D\dot{\alpha} = \tau + M \tag{3.25}$$

where $J \in \mathbb{R}^{4\times4}$ is the diagonal inertia matrix, $D \in \mathbb{R}^{4\times4}$ is the diagonal viscous damping matrix, $\tau \in \mathbb{R}^4$ control input torque to the pad motors, and $M \in \mathbb{R}^4$ is the moment exerted on the pads about the pivot by the pressure field, whose ith element is given by

$$M_i = r^2 \int_{-L/2}^{L/2} \int_{\underline{\theta}_i}^{\overline{\theta}_i} p_i \sin\theta \mathrm{d}\theta \mathrm{d}z, \quad i = 1, 2, 3, 4. \tag{3.26}$$

Note that for the passive bearing, $\tau = 0$ in (3.25). For the active bearing, we used the following "high-gain" velocity feedback loop to ensure that the desired pad angular velocity input (3.24) is applied to the system,

$$\tau = K_\tau \left(u - \dot{\alpha}\right) \tag{3.27}$$

where $K_\tau \in \mathbb{R}^{4\times4}$ is constant, symmetric, and positive definite. We used the bearing system parameters shown in Table 3.1 with initial conditions $q(0) = (0.01, 0.01)$ mm, $\dot{q}(0) = 0$, $\alpha(0) = (1, 1, 1, 1)$ mrad, and $\dot{\alpha}(0) = 0$. The pad mass was chosen to be 0.0935 kg. Further, we set $J = 4.475 \times 10^{-5} I_4$ kg-m^2 and $D = 8 \times 10^{-2} I_4$ kg-m^2/sec. The control gains for the active bearing were set to $K_1 = 10^3 I_2, K_2 = 10^4 I_2$, and $K_\tau = I_4$.

Figures 3.6 and 3.7 show the simulation results for the passive bearing. Specifically, Figure 3.6 shows that after approximately $t = 1.6$ sec the journal reaches a limit cycle about an eccentricity ratio of 0.15 on the negative y axis (i.e., direction of load). The behavior of the pads is shown in Figure 3.7. Note that α_3 converges to a constant angle because it does not support the load. The results for the active bearing are shown in Figures 3.8-3.11. One can see that the active control is able to prevent the limit cycle and make the journal run concentrically after approximately 30 msec. The pad angles are forced to some constant steady-state values necessary to maintaining

the journal running concentrically. The input torques are not necessarily zero in the steady state since they need to compensate for the hydrodynamic moment M on the pads (see τ_4 in Figure 3.11). The pad torques that are 0 in the steady state (see τ_1, τ_2 and τ_3 in Figure 3.11) indicate that the corresponding motors are turned off when the journal runs concentrically. Further, the simple, linear torque-level control law in (3.27) is successful in compensating for the pad tilt dynamics. Finally, it is worth mentioning that the input matrix $G(q(t), \alpha(t))$ had full row rank for all time.

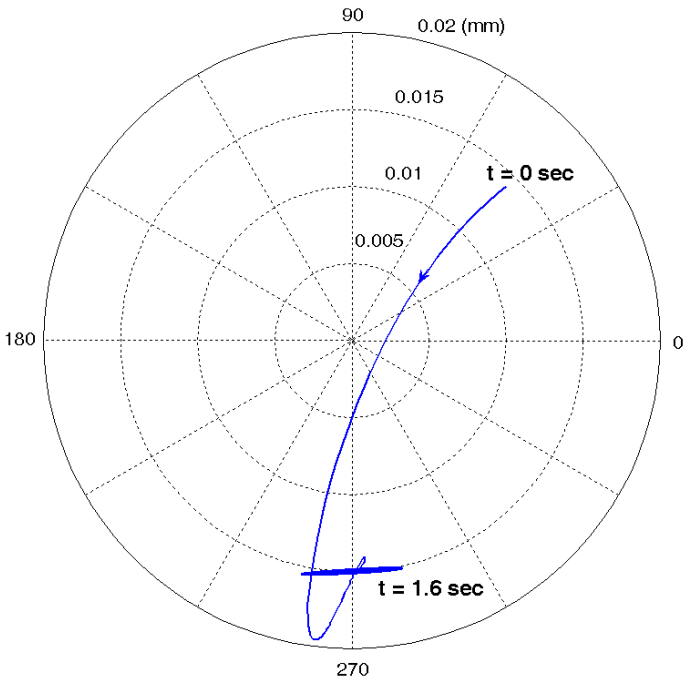

Figure 3.6: Passive bearing: orbit of the journal center q.

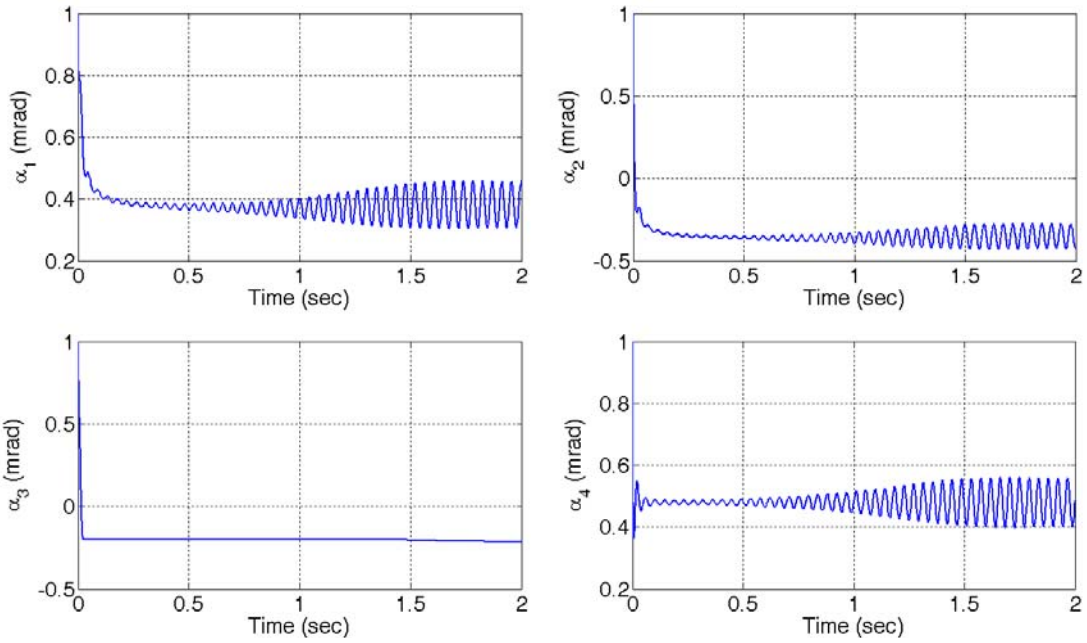

Figure 3.7: Passive bearing: pad tilt angle α.

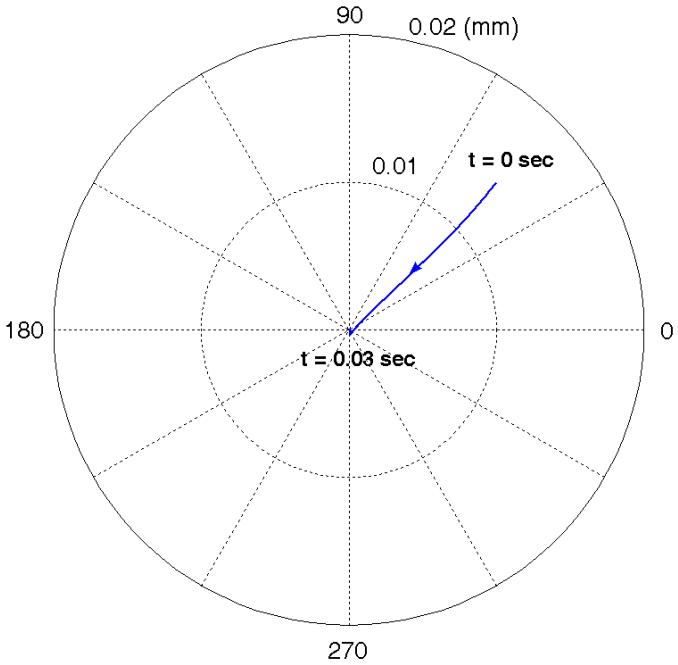

Figure 3.8: Active bearing: orbit of the journal center q.

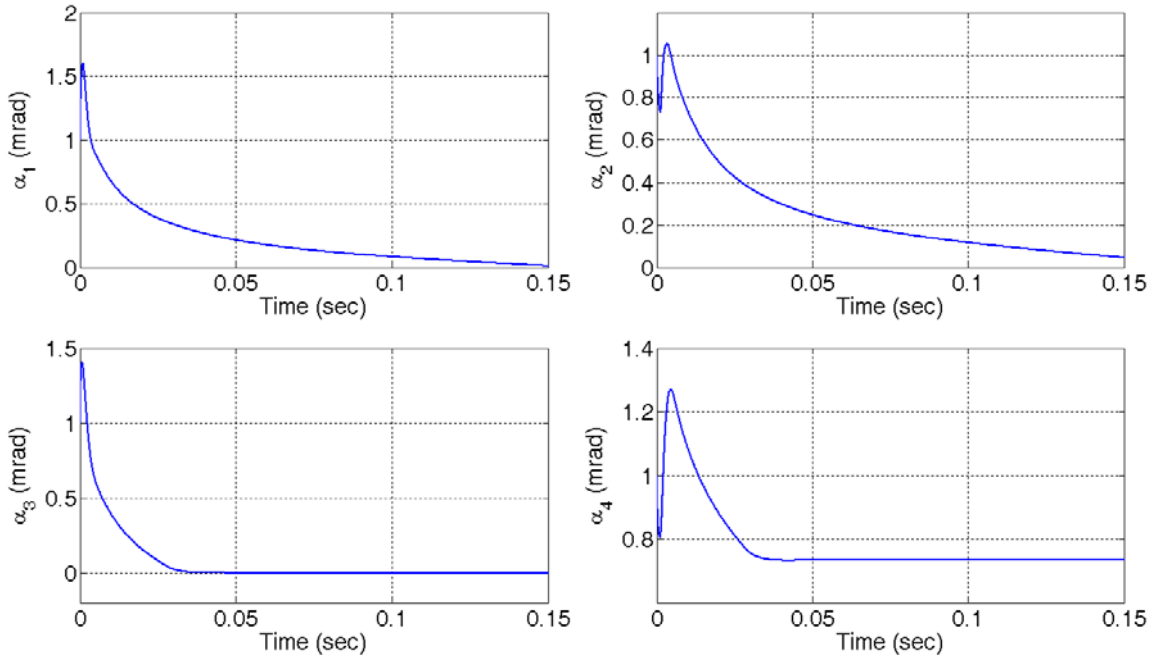

Figure 3.9: Active bearing: pad tilt angle α.

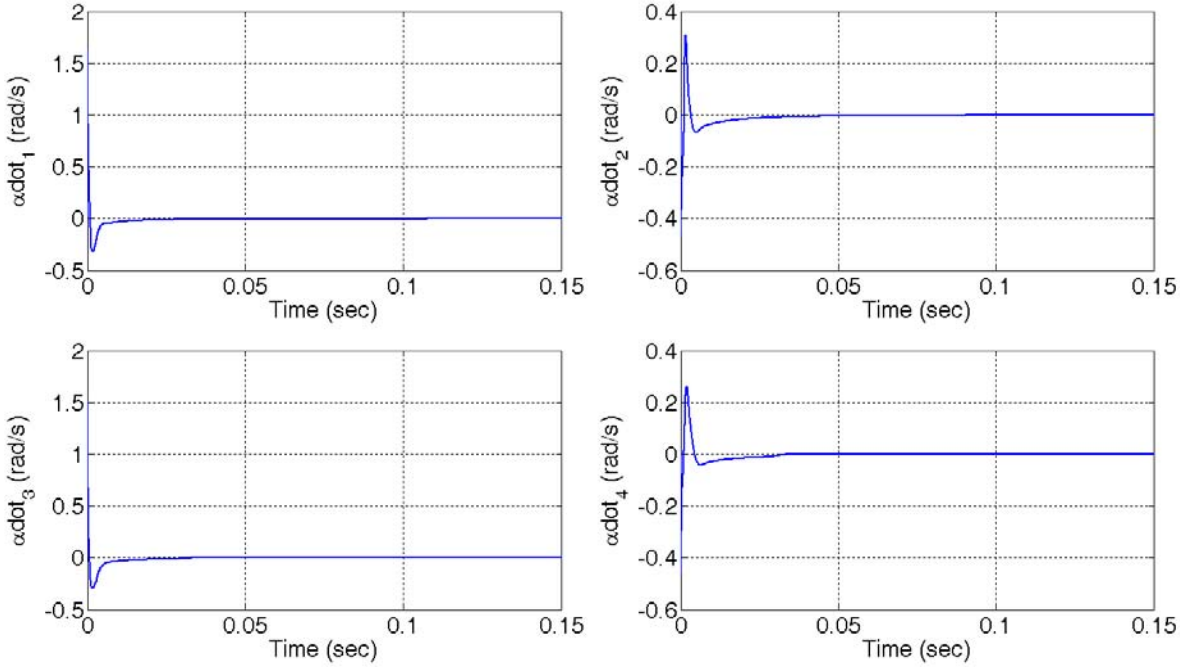

Figure 3.10: Active bearing: pad angular velocity $\dot{\alpha}$.

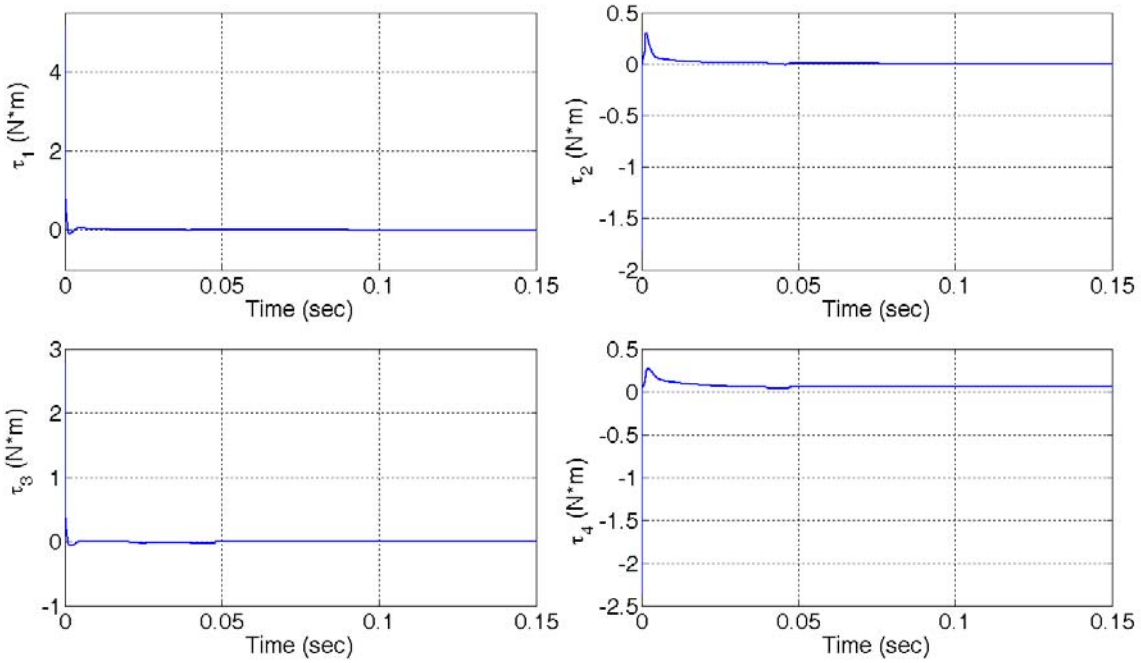

Figure 3.11: Active bearing: input torque τ.

Chapter 4 Conclusions and Future Work

4.1 Conclusions

This dissertation was devoted to the concept of transforming a tilting-pad bearing into an active bearing by actuating the pads via feedback control. Two actuation methods were discussed: the first method relied on radially translating the pads using a linear electric motor (Chapter 2), while the second method actuated the pads along their tilt axis via a rotary electric motor (Chapter 3). The control objective of both actuation methods is the same, viz., to stabilize the journal motion at the center of the bearing clearance. Our results indicated that the second actuation method has potentially more control authority over the journal motion.

The main contributions of the result presented in Chapter 2 are:

► A novel nonlinear model for the hydrodynamic force in the bearing was introduced. That is, rather then using the standard, linear spring-damper type model, we proposed a more realistic hydrodynamic force model that takes the form of a nonlinear squeeze-film damper plus a nonlinear repellent spring.

► A nonlinear feedback control was designed for the proposed nonlinear system model.

► The first ever experimental demonstration of feedback control of an active tilting-pad bearing.

The main contributions of the result presented in Chapter 3 are:

► A new approach for actively operating a tilting-pad bearing was introduced. Instead of actuating the radial position of each pad like in Chapter 2, we proposed to actuate their tilt angles.

► A coupled, nonlinear dynamic model, based on the hydrodynamic force of an infinitely-short bearing, was formulated such that the control inputs were the pad angular velocities.

► A model-based nonlinear control law was designed for the nonlinear system dynamics.

4.2 Recommendations for Future Work

The parameters a_i and b_i in the hydrodynamic force model (2.3) were assumed constant despite their dependency on oil viscosity and rotor speed, which may vary in time. The performance of the proposed model-based controller could be improved by performing a thorough parametric study to determine the exact dependency of a_i and b_i on ω and μ. That is, note that ω is typically measured online to facilitate the control of the rotor speed, while the variation of μ with oil temperature can be determined. Thus, measurements of the rotor speed and oil temperature can be input to the model-based controller to update the values of the parameters a_i and b_i in real time. On the other hand, an alternative approach to deal with uncertainties in ω and μ as well as in the pad tilt angles would be to design an adaptive or robust version of the nonlinear control law (2.10).

The validation of the active pad tilt system in Chapter 3 relied on numerical simulations only. The natural next step for this work is to experimentally test this novel active bearing. Our simulations indicate that the rotary motors for actuating the pads should have a resolution in the sub-milliradians range and a peak torque of a few Newton-meters. Electric motors that satisfy these specifications are commercially available.

References

[1] M.L. Adams and T.H. McCloskey, “A Feasibility and Technology Assessment for the Implementation of Active Rotor Vibration Control Systems in Power Plant Rotating Machinery,” *Proc. Intl. Conf. Rotordynamics*, pp. 327-332, Lyon, France, 1990.

[2] P.E. Allaire, “Design of Journal Bearings for High Speed Rotating Machinery,” *Fundamentals of the Design of Fluid Film Bearings*, New York, NY: ASME, 1979.

[3] Z. Cai, M.S. de Queiroz, and M.M. Khonsari, “Adaptive Control of Active Tilting-Pad Bearings,” *Proc. American Control Conf.*, pp. 2907-2912, Denver, CO, 2003.

[4] Z. Cai, “Nonlinear Control and Its Application to Active Tilting-Pad Bearings,” *Ph.D. Dissertation*, Louisiana State University, Baton Rouge, LA, 2005.

[5] D.C. Deckler, R.J. Villette, F.K. Choy, and M.J. Braun, “Modeling of a Controllable Tilting Pad Bearing,” *Proc. American Control Conf.*, pp. 3416-3420, Albuquerque, NM, 1997.

[6] D.C. Deckler and R.J. Villette, “Simulation and Control of an Active Tilting-Pad Journal bearing,” *Tribology Trans.*, Vol 47, pp. 440-458, 2004.

[7] C.F. Gerald and P.O. Wheatley, *Applied Numerical Analysis*, Boston, MA: Addison-Wesley, 1999.

[8] B.J. Hamrock, *Fundamentals of Fluid Film Lubrication*, New York, NY: McGraw-Hill, 1994.

[9] Khonsari and E.R. Booser, *Applied Tribology – Bearing Design and Lubrication*, New York, NY: John Wiley & Sons, 2001.

[10] M. Krstic, I. Kanellakopoulos, and P. Kokotovic, *Nonlinear and Adaptive Control Design*, New York, NY: John Wiley & Sons, 1995.

[11] J.W. Lund, “Spring and Damping Coefficients for the Tilting-Pad Journal Bearing,” *ASLE Trans.*, Vol. 7, pp. 342-352, 1964.

[12] E.P. Okabe and K.L. Cavalca, “Rotordynamic Analysis of Systems with a Non-Linear Model of Tilting Pad Bearings Including Turbulence Effects,” *Nonlinear Dyn.*, published online on June 28, 2008.

[13] I.F.Santos, “On the Adjusting of the Dynamic Coefficients of Tilting-Pad Journal Bearings,” *Tribology Trans.*, Vol. 38, No. 3, pp. 700-706, 1995.

[14] H. Ulbrich and J. Althaus, “Actuator Design for Rotor Control,” *ASME Design Technical Conf.: Proc. 12th Biennial Conf. Mechanical Vibration and Noise*, pp. 17-22, Montreal, Canada, 1989.

[15] F.Y. Zeidan, “Developments in Fluid Film Bearing Technology,” *Turbomachinery Intl.*, pp. 24-31, Sept./Oct. 1992.

[16] A. Ben-Israel and T.N.E. Greville, *Generalized Inverses: Theory and Applications*, New York: Springer-Verlag, 2003.

[17] K.S. Narendra and A.M. Annaswamy, *Stable Adaptive Systems*, Mineola, NY: Dover, 2005.

[18] A. Wu, Z. Cai, and M.S. de Queiroz, "Model-Based Control of Active Tilting-Pad Bearings," *IEEE/ASME Trans. Mechatronics*, Vol. 12, No. 6, pp. 689-695, 2007.

Vita

An Wu was born in Chongqing, People's Repubic of China. He received a Bachelor of Science Degree in Electrical Engineering from Huazhong University of Science and Technology, Wuhan, P.R.China, in June 2006. Since August 2006, he has been a doctoral student in the Department of Mechanical Engineering of Louisiana State University, Baton Rouge, Louisiana. He worked with Dr. Marcio de Queiroz as a research assistant, focusing on the dynamic modeling and feedback control of active fluid film bearings.